

Guy G. Campbell  
Vice President - Nuclear

419-321-8588  
Fax: 419-321-8337

Docket Number 50-346

License Number NPF-3

Serial Number 2700

April 23, 2001

United States Nuclear Regulatory Commission  
Document Control Desk  
Washington, D.C. 20555-0001

Subject: Submittal of ASME Code Case N-481 Evaluation for the Davis-Besse Nuclear Power  
Station Reactor Coolant Pumps

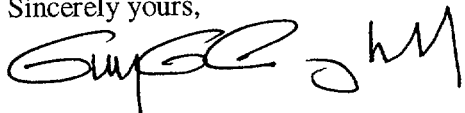
Ladies and Gentlemen:

The purpose of this letter is to submit the attached Davis-Besse Nuclear Power Station (DBNPS) report, "ASME Code Case N-481 Evaluation of Davis-Besse Reactor Coolant Pumps," for NRC review as required by Code Case N-481. This report demonstrates the safety and serviceability of the DBNPS Reactor Coolant Pump (RCP) casings using the criteria of American Society of Mechanical Engineers (ASME) Boiler & Pressure Vessel (B&PV) Code Case N-481, "Alternative Examination Requirements for Austenitic Pump Casings." Code Case N-481 has been endorsed by the NRC in Regulatory Guide 1.147, "Inservice Inspection Code Case Acceptability - ASME Section XI, Division 1," Revision 12. This Code Case has been incorporated into the DBNPS Inservice Inspection Program and was utilized during the 12<sup>th</sup> refueling outage conducted in the spring of 2000 for inspection of the RCP casings.

Attachment 2 provides the listing of commitments identified in this document. There are no commitments made by the DBNPS in this document.

Should you have any questions or require additional information, please contact Mr. David H. Lockwood, Manager-Regulatory Affairs, at (419) 321-8450.

Sincerely yours,



RMC/dlc

Attachment

A047

Docket Number 50-346  
License Number NPF-3  
Serial Number 2700  
Page 2

cc: J. E. Dyer, Regional Administrator, NRC Region III  
S. P. Sands, DB-1 NRC/NRR Project Manager  
K. S. Zellers, DB-1 Senior Resident Inspector  
Utility Radiological Safety Board  
Ohio Department of Commerce – Industrial Compliance

Docket Number 50-346  
License Number NPF-3  
Serial Number 2700  
Attachment 1

**ASME Code Case N-481**  
**Evaluation of Davis-Besse Reactor Coolant Pumps**

(74 Pages Follow)

Report No.: SIR-99-040  
Revision No.: 1  
Project No.: TECO-07Q  
File No.: TECO-07Q-401  
September 2000

**ASME Code Case N-481  
Evaluation of Davis-Besse Reactor Coolant Pumps**

*Prepared for:*

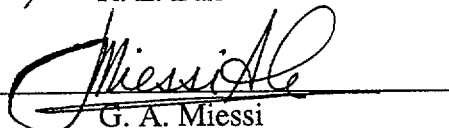
Toledo Edison Company

*Prepared by:*

Structural Integrity Associates, Inc.  
San Jose, California

*Prepared by:*   
R. L. Bax

Date: 9/27/00

*Prepared by:*   
G. A. Miessi

Date: 9/27/00

*Reviewed and  
Approved by:*   
N. G. Cofie

Date: 9/27/00



**Structural Integrity Associates, Inc.**

## REVISION CONTROL SHEET

Document Number: SIR-99-040

Title: ASME Code Case N-481 Evaluation of Davis-Besse Reactor Coolant Pumps

Client: Toledo Edison Company

SI Project Number: TECO-07Q

Section	Pages	Revision	Date	Comments
-	-	A	7/30/99	Draft Issue
-	i - v	0	10/8/99	Initial Issue
1.0	1-1 – 1-7			
2.0	2-1			
3.0	3-1 – 3-2			
4.0	4-1 – 4-53			
5.0	5-1			
6.0	6-1 – 6-3			
App. A	A-0 – A-1			
-	i, iv	1	09/26/00	Incorporated Client's Comments
1.0	1-4			
4.0	4-11, 4-15, 4-35			



## Table of Contents

<u>Section</u>	<u>Page</u>
1.0 INTRODUCTION.....	1-1
1.1 Background .....	1-1
1.2 Description of Reactor Coolant Pump Casings at Davis-Besse.....	1-1
1.3 Objective and Organization.....	1-3
2.0 PREVIOUS INSPECTIONS.....	2-1
3.0 BACKGROUND ON ASME CODE CASE N-481 .....	3-1
4.0 ASME CODE CASE N-481 EVALUATION .....	4-1
4.1 Evaluation of Material Properties, Including Fracture Toughness .....	4-1
4.2 Stress Analysis Results.....	4-9
4.3 Review of Operating History of the Pumps .....	4-10
4.4 Selection of Locations for Postulating .....	4-11
4.5 Postulated Flaw .....	4-11
4.6 Determination of Stability of Postulated Flaw .....	4-11
4.7 Effect of Thermal Embrittlement and Other Degradation Mechanisms that May Degrade Properties of the Pump Casing .....	4-16
5.0 SUMMARY AND CONCLUSIONS.....	5-1
6.0 REFERENCES.....	6-1



## List of Tables

<u>Table</u>	<u>Page</u>
Table 1-1    Design and Functional Requirements of Davis-Besse Reactor Coolant Pumps [4] .....	1-4
Table 4-1    Determination of Lower Bound Fracture Toughness of Davis-Besse Pump Casings Considering Thermal Embrittlement .....	4-17
Table 4-2    Determination of Lower Bound Fracture Toughness of Davis-Besse Pump Casings Welds Considering Thermal Embrittlement .....	4-18
Table 4-3    Summary of Stresses .....	4-24
Table 4-4    Thickness and Flaw Dimensions at Postulated Flaw Locations .....	4-25
Table 4-5    Comparison of Calculated and Allowable Stress Intensity Factors .....	4-26
Table 4-6    Fatigue Crack Growth Evaluation Results .....	4-28



## List of Figures

<u>Figure</u>	<u>Page</u>
Figure 1-1. Davis-Besse Reactor Coolant Pump Assembly [4].....	1-5
Figure 1-2. Davis-Besse Reactor Coolant Pump Casing Regions .....	1-6
Figure 1-3. Schematic Drawing Showing Davis-Besse Reactor Coolant Pump Casing Welds.....	1-7
Figure 4-1. Effect of Thermal Aging on Room Temperature Impact Energy of CF3, CF8 and CF8M Cast Stainless Steel [15].....	4-29
Figure 4-2. Microstructure of Solution Heat Treated Wrought Type 316 Stainless Steel.....	4-30
Figure 4-3. Microstructure of Solution Heat Treated Grade CF8 Stainless Steel Casting .....	4-31
Figure 4-4. Effect of Temperature on Charpy Transition Curves of CF3, CF8 and CF8M Steels Aged for 30,000 hours [15] .....	4-32
Figure 4-5. Flow Diagram for Estimating Mechanical Properties of Aged Cast Stainless Steels in LWR Systems [21] .....	4-33
Figure 4-6. Example of a Typical J-R Curve and Determination of $J_{Ic}$ Using the ASTM E 813-81 Methodology [14].....	4-34
Figure 4-7. Determination of $J_{Ic}$ for Davis-Besse Reactor Coolant Pump 1A1 Casing.....	4-35
Figure 4-8. Determination of $J_{Ic}$ for Davis-Besse Reactor Coolant Pump 1A2 Casing.....	4-36
Figure 4-9. Determination of $J_{Ic}$ for Davis-Besse Reactor Coolant Pump 1B1 Casing.....	4-37
Figure 4-10. Determination of $J_{Ic}$ for Davis-Besse Reactor Coolant Pump 1B2 Casing.....	4-38
Figure 4-11. Flow Stress Ratio of Aged Cast Stainless Steels at Room Temperature as a Function of Normalized Aging Parameter [21].....	4-39
Figure 4-12. Flow Stress Ratio of Aged Cast Stainless Steels at 290 C as a Function of Normalized Aging Parameter [21] .....	4-40
Figure 4-13. Dimensions Used for Finite Element Model for Davis-Besse Pump Casings (Part 1).....	4-41
Figure 4-14. Dimensions Used for Finite Element Model for Davis-Besse Pump Casings (Part 2).....	4-42
Figure 4-15. Dimensions Used for Finite Element Model for Davis-Besse Pump Casings (Part 3).....	4-43
Figure 4-16. Overall Finite Element Model for Davis-Besse Pump Casings (Part 1) .....	4-44
Figure 4-17. Overall Finite Element Model for Davis-Besse Pump Casings (Part 2) .....	4-45
Figure 4-18. Stress Intensity Distribution Due to Internal Pressure of 2250 psig .....	4-46
Figure 4-19. Critical Temperature Distribution During Heatup .....	4-47
Figure 4-20. Critical Stress Distribution During Heatup .....	4-48
Figure 4-21. Critical Temperature Distribution During Cooldown .....	4-49
Figure 4-22. Critical Stress Distribution During Cooldown .....	4-50
Figure 4-23. Results of Fatigue Crack Growth Analysis for Davis-Besse Pump Casing.....	4-51
Figure 4-24. Critical Path Locations (1 of 2) .....	4-52
Figure 4-25. Critical Path Locations (2 of 2) .....	4-53





## **1.0 INTRODUCTION**

### **1.1 Background**

ASME Boiler and Pressure Vessel Code, Section XI requires periodic inservice inspection of various nuclear power plant components. Specifically, inservice inspection requirements of pressure retaining welds of pump casings (Category B-L-1) are delineated in Table IWB-2500-1 of the Code. The requirements call for periodic visual and volumetric examinations of the weldments using radiography or ultrasonic inspection (UT). Inservice inspection of cast stainless steel pump casings using radiography or UT has proved to be a very difficult challenge in the nuclear industry. In recognition of this difficulty, alternate examination requirements have been provided in Code Case N-481 [1], shown in Appendix A of this document. These alternate requirements consist of visual inspections and an analytical evaluation to demonstrate the safety and serviceability of the pump casings in the presence of an assumed flaw. Toledo Edison Company has opted to invoke Code Case N-481 in application to the reactor coolant pumps (RCPs) at Davis-Besse. This document addresses the analytical aspect of Code Case N-481 as it applies to the RCPs at Davis-Besse.

### **1.2 Description of Reactor Coolant Pump Casings at Davis-Besse**

Davis-Besse employs four RCPs to circulate coolant through the reactor coolant system. Davis-Besse has a two loop configuration with two pumps per loop. All four pumps (P1A1 (TECO 1-2-1), P1A2 (TECO 1-2-2), P1B1 (TECO 1-1-1) and P1B2 (TECO 1-1-2)) consist of vertical, single-stage, bottom suction, horizontal-discharge, centrifugal-diffuser-casing units classified as Type E in ASME Code, Section III, Subsubarticle NB-3400. All four pumps were manufactured by the Byron Jackson Pump Division of the Borg-Warner Corporation (now Flowserve). The pumps were designed to the requirements of the 1968 Edition of Section III of the ASME Boiler and Pressure Vessel Code [2] to Class A (Class 1) Nuclear Vessels, for nuclear service, using specifications provided by Babcock and Wilcox [3].

A schematic of the pump assembly is shown in Figure 1-1 [4]. As can be seen from this figure, the assembly is comprised of the following components:

- a) motor
- b) driver mount
- c) rotating element (coupling, impeller and shaft)
- d) heat exchanger
- e) seal cartridge (and mechanical seals)
- f) cover
- e) casing

The assembly is supported by the discharge and suction nozzle piping, and four hanger brackets attached to the pump case. Some of the design and functional requirements of the pump are shown in Table 1-1. As stated above, Code Case N-481 applies only to the pressure-retaining welds of the pump casings. The inspection requirements for all other components are unaffected by this Code Case.

The four reactor coolant pump casings at Davis-Besse were fabricated from ASTM A351, Grade CF8M cast austenitic stainless material. Figure 1-2 identifies the various portions of the pump casing. At the bottom of the pump casing is the suction nozzle whose axis of symmetry is an extension of the axis of rotation of the pump shaft. The lower flange occupies the upper end of the suction nozzle, and is marked by a series of internal steps as shown in Figure 1-2. The upper end of the lower flange blends into the diffuser. The diffuser consists of upper and lower rings separated by vanes. The upper diffuser ring blends into the upper flange. All portions previously described make up the hub. The scroll (volute) section is a relatively thin-walled section connecting the upper and lower flanges outside of the diffuser. The scroll forms a spiral around the diffuser as shown in Figure 1-2, starting at the crotch area and terminating at the discharge nozzle.

During fabrication, the volute and the hub sections were cast independently. They were then welded together. As shown in Figure 1-3, there are two horizontal welds that join the hub and scroll portions of the pump casing (one on the upper end and the other on the lower end). These two welds are joined together by a circumferential or vertical weld near the crotch region. The casings were inspected by radiography for fabrication-related defects such as slag inclusions, voids and cracks. Indications exceeding acceptance standards were repaired [5a, 5b]. Following all repairs, the casings were solution heat treated.

### **1.3 Objective and Organization**

The objective of this document is to address the safety and serviceability requirements of ASME Code Case N-481 for the RCPs at Davis-Besse to assure that postulated flaws in the pump casings at critical locations will be stable, considering the operating stresses and material properties of the pump casings. Section 2 of this report discusses previous inspections that have been performed on the pump casings, and the inspection results. Section 3 discusses the background of Code Case N-481, the items covered by the ASME Code Case, and the safety factors used with this Code Case. Section 4 provides the specific evaluation performed using this Code Case. Section 5 presents the conclusions of the evaluation, and Section 6 provides the references used in the evaluation.



Table 1-1

Design and Functional Requirements of  
Davis-Besse Reactor Coolant Pumps [4]

Design Life	40 years
Design Pressure	2,500 psia
Design Temperature	650 F
Operating Pressure	2,250 psia
Operating Temperature	557 F
Rated Flow	88,000 gpm
Rotating Speed	900 rpm

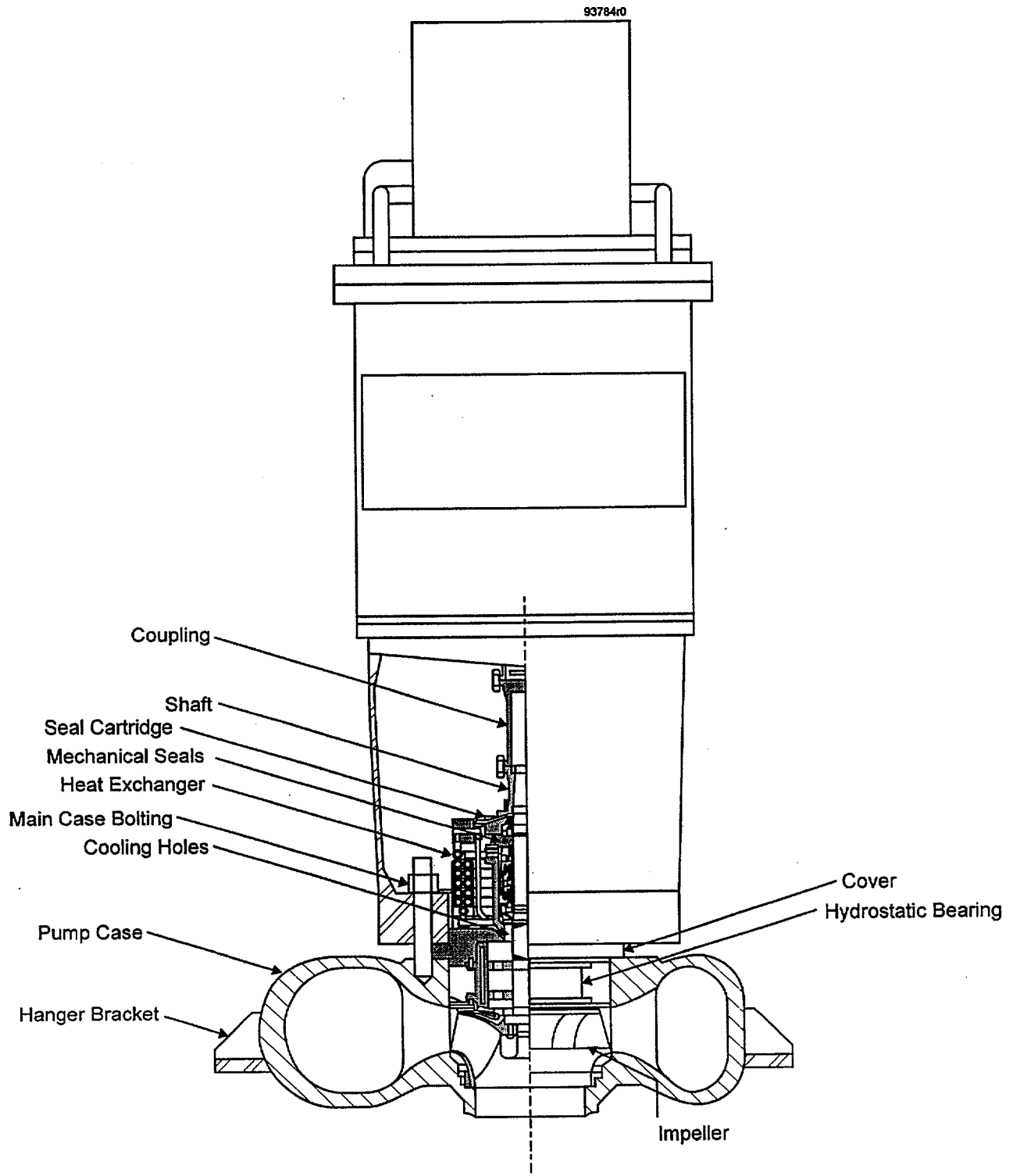


Figure 1-1. Davis-Besse Reactor Coolant Pump Assembly [4]

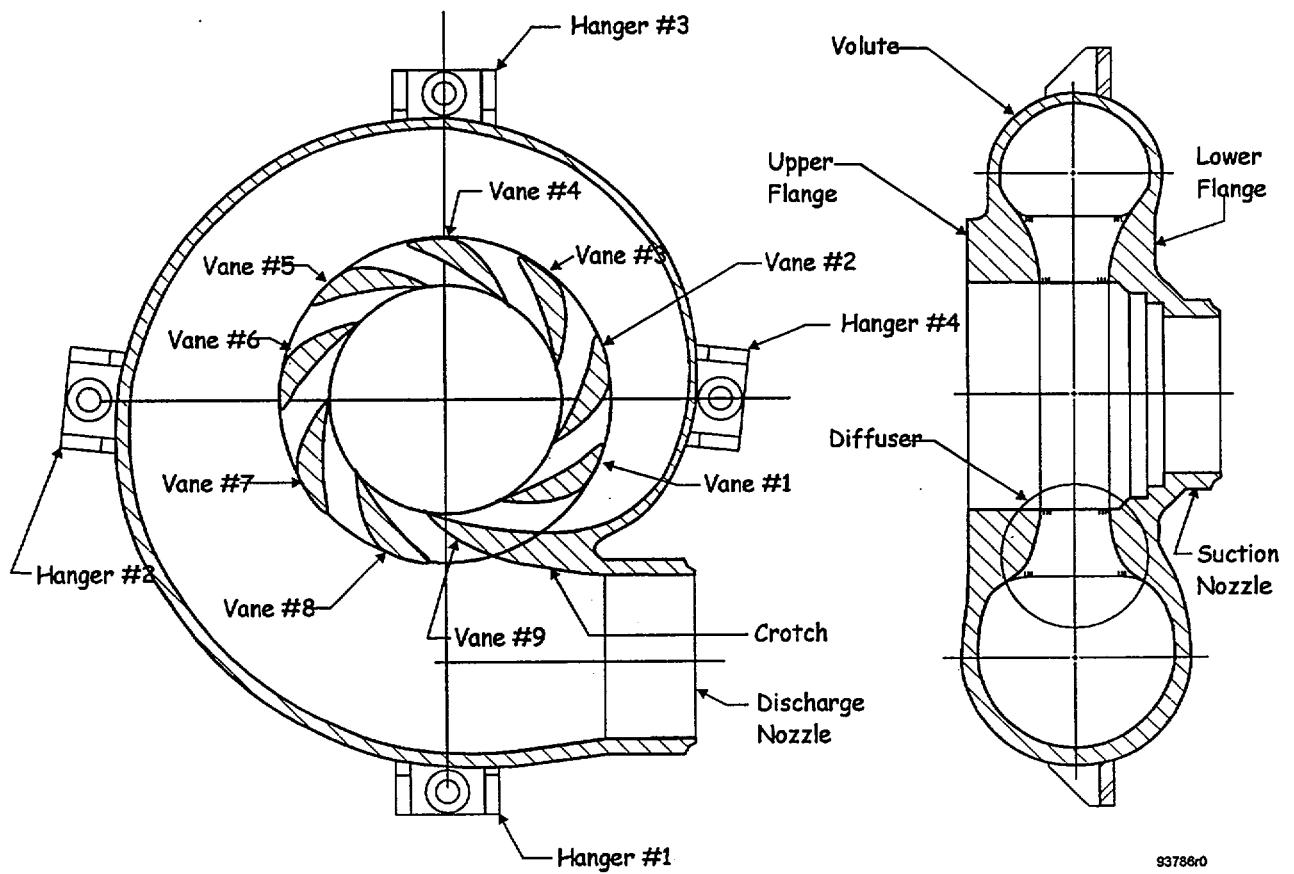


Figure 1-2. Davis-Besse Reactor Coolant Pump Casing Regions

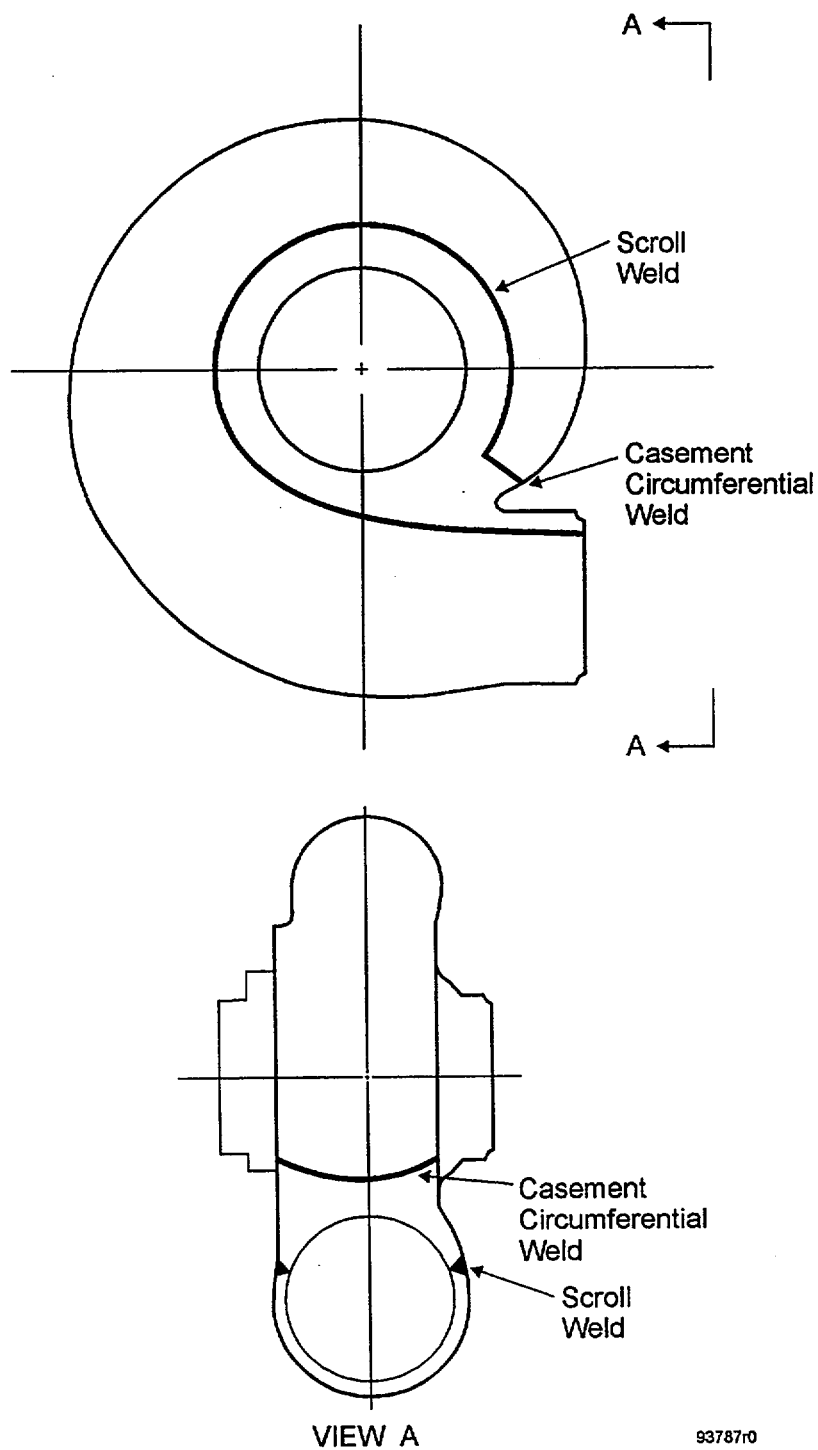


Figure 1-3. Schematic Drawing Showing Davis-Besse Reactor Coolant Pump Casing Welds

## 2.0 PREVIOUS INSPECTIONS

Baseline examinations were performed on all four pump casing after fabrication [5a]. All relevant indications identified during the inspections which exceeded the acceptance standards were repaired [5b]. The pump casing was solution heat treated after the repairs to ensure that local weld residual stresses resulting from the repairs were minimized.

Volumetric examinations consisting of radiographic techniques (RT) and ultrasonic techniques (UT) were performed on Pump P1A1 (TECO 1-2-1) during refueling outage 6 in 1990 [6]. Double-wall RT technique was used for examining 85% of the upper and lower scroll welds. RT could not be used on the remaining 15% of the upper and lower scroll welds and the entire torus weld due to internal radiation scattering and geometrical constraints. As such, they were examined using UT. No indications were observed during these examinations.





### 3.0 BACKGROUND ON ASME CODE CASE N-481

A review of data collected in EPRI's "Cast Austenitic Stainless Steel Sourcebook" [7] shows that fabrication-related defects, such as slag inclusions and porosity, are not uncommon during the manufacturing process. However, whenever such defects are identified by surface or volumetric inspection during fabrication, they are usually excavated and weld repaired. Examinations and repairs during the fabrication process are accomplished with relative ease, since they are performed in a shop environment.

Ultrasonic examination and radiography of pump casings, once in service, are very difficult and time consuming. As noted by the NRR in response to a previous Relief Request by a sister plant, and the subsequent Safety Evaluation [8], the disassembly of a reactor coolant pump for the sole purpose of performing a volumetric examination of the pump casing welds is not practical. There is considerable personnel radiation exposure and significant outage time associated with removal of the pump shaft. Industry operating experience with cast stainless steel pressure components has been good. Furthermore, no detrimental service induced degradation of pump casing welds, detected with various inspection techniques, has been reported.

Because of the difficulties associated with the examination of pump casing welds after being placed in service, ASME Code Case N-481 (shown in Appendix A) addresses alternate examinations and evaluations that may be performed in lieu of the volumetric examinations specified in Table IWB-2500-1 of Section XI, Division 1 of the ASME Code for Examination Category B-L-1. Examination Category B-L-1 relates to pressure retaining welds in pump casings; hence, the application of this code case is limited to the scroll welds, the vertical welds, and the adjacent base metal. The internal diffuser vanes, their attachment welds, and other attachment welds, which are not pressure retaining, are, therefore, excluded from this evaluation.



In addition to performing visual examinations (VT-1, VT-2 and VT-3), the code case outlines a seven-step evaluation procedure to demonstrate the safety and serviceability of the pump casings. Key to this procedure is the demonstration that an assumed quarter-thickness flaw, with length six times its depth, will remain stable, considering the stresses and material properties (base and weld materials) of the pump casings.

The ASME Code Case N-481 evaluation procedure is very similar to that in Appendix G of Sections III and XI of the ASME Code, which provides fracture toughness criteria for protection against failure of reactor pressure vessels, in that a similar postulated flaw is assumed for the analysis in both cases. The Code Case does not provide any guidance on safety factors to be used in the evaluation. Therefore, for the evaluation presented herein, safety factors consistent with Appendix G for similar evaluations of pressure vessels have been used.

Although Code Case N-481 does not require a fatigue crack growth evaluation, and such analyses are not part of an Appendix G evaluation of the stability of a quarter-thickness deep flaw, calculations are done in this study to demonstrate that a small initial assumed flaw will not reach the quarter-thickness flaw during plant life.



## **4.0 ASME CODE CASE N-481 EVALUATION**

In this section, the seven items listed in the Code Case are addressed in relation to Davis-Besse in order to demonstrate the safety and serviceability of pump casings.

### **4.1 Evaluation of Material Properties, Including Fracture Toughness**

The pump casing material conforms to ASTM A351, Grade CF8M, which is an austenitic stainless steel casting specification. A review of the fabrication records indicates that during the fabrication process, the pump casing welds were made using either the shielded metal arc welding (SMAW) or submerged arc welding (SAW) process. The records also show that several weld repairs were performed during fabrication. After welding, the casings were solution heat treated at 1900-2050°F for ten hours, followed by rapid cooling (agitated quenching in water to a temperature at or below 700°F within five minutes).

The most important material property pertinent to this evaluation is the fracture toughness. The fracture toughness of the base material and the weld metal are addressed separately since they are affected by different mechanisms.

#### **4.1.1 *Fracture Toughness of ASTM A351, Grade CF8M***

The fracture toughness of cast austenitic stainless steels has been the subject of significant research in the U.S. and elsewhere in recent years. Three grades of cast austenitic stainless steel frequently used in nuclear power plant applications (CF3, CF8 and CF8M) have all been studied extensively to determine the kinetics and material parameters that control the toughness of these materials. The major conclusion drawn from most of the work done on these castings is that unaged cast austenitic stainless steels have relatively high toughness values. However, during service at LWR operating temperatures, they become embrittled with time, which results in a loss of toughness as shown in Figure 4-1.

The microstructure of stainless steel castings is significantly different from that of wrought products. Wrought products consist of a single phase, austenite ( $\gamma$ ), as shown in Figure 4-2. Castings, on the other hand, exhibit a two-phase, or "duplex," microstructure of austenite ( $\gamma$ ) and delta ferrite ( $\delta$ ), as shown in Figure 4-3. The ferrite phase in the duplex structure in these castings increases the tensile strength, improves the weldability and soundness of the casting, and increases the resistance to stress corrosion cracking. However, various carbide phases, intermetallic compounds such as sigma and chi phases, and a chromium rich bcc phase ( $\alpha'$ ) can precipitate in the ferrite phase during service and lead to substantial degradation in toughness properties. Research performed at the Argonne National Laboratory (ANL) and elsewhere [9 through 21] has shown that thermal embrittlement of cast stainless steel components will occur during the reactor design lifetime of 40 years.

As a result of such thermal aging embrittlement, the Charpy transition curve shifts to higher temperatures as shown in Figure 4-4. For cast stainless steel of all grades, the extent of thermal embrittlement increases with an increase in ferrite content. The low-carbon CF3 grades are the most resistant and the molybdenum-bearing high carbon CF8M grades are the least resistant to thermal embrittlement.

The embrittlement of cast stainless steels results in brittle fracture associated with either the cleavage of the ferrite or separation of the ferrite/austenite phase boundaries. The degree of embrittlement is controlled by the amount of delta ferrite and the extent of ferrite/austenite phase boundaries. Brittle failure occurs either when the ferrite phase is continuous, as is the case with high-ferrite cast material, or when the ferrite/austenite phase boundaries provide an easy path for crack propagation. Hence, the amount, size and distribution of the ferrite phase in the duplex microstructure and the presence of phase boundary carbides are important parameters in controlling the extent of thermal embrittlement.

The kinetics of thermal embrittlement have been explained in detail by Chopra, et al, [9 through 13]. The kinetics are controlled by several mechanisms that depend on material parameters and aging temperatures. During long term exposure at elevated temperature,



additional phases are precipitated in the ferrite matrix. These include the formation of a chromium (Cr) - rich  $\alpha'$  phase by spinodal decomposition; nucleation and growth of  $\alpha'$ ; precipitation of nickel (Ni) - and silicon (Si) -rich G phase,  $M_{23}C_6$  carbide and  $\gamma_2$  (austenite); and additional precipitation and/or growth of existing carbides at the ferrite/austenite phase boundaries.

The chemical composition of the casting and the ferrite morphology are important parameters that influence embrittlement. A procedure and correlations for predicting the fracture toughness of aged, cast stainless steels from known material information is provided by Chopra [21]. The methodology for determining the fracture toughness of cast stainless steels, considering embrittlement, is summarized in the flow chart of Figure 4-5 (extracted from Reference 21). The approach consists of determining the ferrite content of the cast stainless steel from known chemical composition as stated on CMTRs. From the ferrite content, the minimum impact energy is calculated, and the material resistance J-R curve is determined. An estimate of the fracture toughness,  $J_{Ic}$ , is then obtained from the J-R curve.

The only information required in these correlations is the chemical composition from the certified material test report (CMTR). A correlation for the extent of thermal embrittlement at "saturation" (the minimum impact energy that would be achieved for the material after long term aging at a given operating temperature) is given in terms of the chemical composition. The extent of thermal embrittlement as a function of time and temperature of reactor service is then estimated from the extent of embrittlement at saturation and from the correlations describing the kinetics of embrittlement, which are also given in terms of the chemical composition. In this evaluation, the fracture toughness associated with the minimum impact energy at an aging temperature of 550°F) will be conservatively used.

Using the methodology of Reference 21, the chromium equivalent ( $Cr_{eq}$ ) and nickel equivalent ( $Ni_{eq}$ ) are determined from the chemical composition, based on Hull's equivalent factors [22]:

$$Cr_{eq} = (Cr) + 1.21 (Mo) + 0.48 (Si) - 4.99 \quad (4-1)$$

$$Ni_{eq} = (Ni) + 0.11 (Mn) - 0.0086 (Mn)^2 + 18.4 (N) + 24.5 (C) + 2.77 \quad (4-2)$$

where the chemical composition is in wt%. Per Reference 21, the value of N is assumed to be 0.04 if it is not available on the CMTR.

The ferrite content ( $\delta_c$ ) is then estimated from the relationship:

$$\delta_c = 100.3 (Cr_{eq}/Ni_{eq})^2 - 170.72 (Cr_{eq}/Ni_{eq}) + 74.22 \quad (4-3)$$

For CF8M cast stainless steel, the saturation (minimum) impact energy ( $Cv_{sat}$ ) considering thermal embrittlement can be determined by two methods:

In the first method, the material parameter  $\Phi$  is calculated from which  $Cv_{sat}$  is determined as follows:

$$\Phi = \delta_c (Ni + Si + Mn)^2 (C + 0.4N) / 5. \quad (4-4)$$

The saturation value of RT impact energy,  $Cv_{sat}$ , for steels with < 10% Ni is given by

$$\text{Log}_{10} Cv_{sat} = 1.10 + 2.12 \exp(-0.041 \Phi). \quad (4-5)$$

And for steels with >10% Ni by

$$\text{Log}_{10} Cv_{sat} = 1.10 + 2.64 \exp(-0.064 \Phi). \quad (4-6)$$

In the second method,  $Cv_{sat}$  is estimated directly from the chemical compositions of the steel and is given by:

$$\begin{aligned} \text{Log}_{10} Cv_{sat} = & 7.28 - 0.011 (\delta_c) - 0.185 (Cr) - 0.369 (Mo) - 0.451 (Si) \\ & - 0.007 (Ni) - 4.71 (C + 0.4N) \end{aligned} \quad (4-7)$$



The saturation impact energy is determined using both methods given in Equations 4-5/4-6 and 4-7 and the lower value is used for estimating the fracture toughness.

The material resistance J-R curve can be estimated from  $Cv_{sat}$  using a power law relationship:

$$J_d = C [Cv_{sat}]^m [\Delta a]^n \quad (4-8)$$

where:  $J_d$  is the deformation J-Integral ( $\text{kJ/m}^2$ ) per ASTM Specification E813-85  
 $\Delta a$  is the crack extension (mm)  
 $C$  is a constant  
 $m, n$  are power law exponents

The saturation fracture toughness J-R curve at room temperature for static-cast CF8M stainless steel is given by [21]:

$$J_d = 16 [Cv_{sat}]^{0.67} [\Delta a]^n \quad (4-9)$$

In English units, the J-R curve (units of  $J$  in in-kips/in<sup>2</sup> and  $\Delta a$  in inches) is given by:

$$J_d = 91 [25.4]^n [Cv_{sat}]^{0.67} [\Delta a]^n \quad (4-10)$$

The value of  $n$  at room temperature is given by:

$$n = 0.25 + 0.077 \log_{10} Cv_{sat} \quad (4-11)$$

Corresponding equations for the J-R curve at temperatures between 290°C and 320°C (554°F and 608°F) are given by:



$$J_d = 49[Cv_{sat}]^{0.41} [\Delta a]^n \text{ (SI units)} \quad (4-12)$$

$$J_d = 280[25.4]^n [Cv_{sat}]^{0.41} [\Delta a]^n \text{ (English units)} \quad (4-13)$$

$$n = 0.23 + 0.057 \log_{10} Cv_{sat} \quad (4-14)$$

The above equations for the J-R curve can be expressed in simple terms as:

$$J_d = C [\Delta a]^n \quad (4-15)$$

The calculation of all the above parameters, including C and n for the scroll, hub and the attachments for the four RCP casings at Davis-Besse, are shown in Tables 4-1 through 4-2. The CMTRs used in the determination of the parameters in Tables 4-1 through 4-2 were obtained from Reference 23.

The above correlations (Equations 4-1 through 4-15) account for degradation of toughness due to thermal aging, but do not explicitly consider the initial fracture properties of the original unaged material. Fracture toughness data in Reference 21 indicate that the J-R curve for some heats of unaged cast stainless steel may be lower than those for wrought stainless steel. To take into account the possibility of a relatively low initial unaged toughness, the methodology outlined in Figure 4-5 requires that the saturation J-R curves be compared to the lower bound J-R curve for the unaged cast stainless steel. The lower of the two curves is then used. For static cast stainless steel, the lower bound unaged J-R curve is given by:

$$J_d = 400 [\Delta a]^{0.40} \text{ (SI units)} \quad (4-16)$$

$$J_d = 8330 [\Delta a]^{0.4} \text{ (English units)} \quad (4-17)$$





The value of the fracture toughness,  $J_{Ic}$ , can be estimated from the J-R curve using the method outlined in ASTM Specification E813-85 [24]. This ASTM methodology is illustrated in Figure 4-6. In this figure, the line emanating from the origin, or the blunting line, is given by  $J = 2\sigma_f\Delta a$ , where  $\sigma_f$  is the flow stress (the average of the 0.2% offset yield strength and the ultimate tensile strength). Two exclusion lines are constructed parallel to the blunting line but offset by 0.15mm (0.006 in.) and 1.5 mm (0.06 in.). In the ASTM method where the J-R curve is determined by test, a straight line is fit to the test data between the 0.15mm and 1.5mm exclusion lines. This line is extrapolated back to the blunting line and the intersection is termed  $J_Q$ .  $J_{Ic}$  equals  $J_Q$  if various validity criteria are satisfied. In this study, where the J-R curve is established based on material properties and not on test data, a modified form of the ASTM E813 method suggested by Hiser [14] for thermally-aged cast stainless steels is used. In this modified procedure,  $J_{Ic}$  is defined as the intersection of the power law J-R curve with the 0.15mm exclusion line. Comparison of this methodology with the ASTM E813 methodology in [14] for aged cast stainless steels has shown that both methods yield nearly identical  $J_{Ic}$  values.

Determination of  $J_{Ic}$  values for the four pumps are shown in Figures 4-7 through 4-10. In constructing the blunting lines in Figures 4-7 through 4-10, the values of the yield and ultimate tensile strengths are required in order to determine the flow stress. The yield and ultimate tensile strength values are provided at room temperature in the CMTRs from Reference 23, and shown in Tables 4-1 through 4-2. The yield and ultimate tensile strength values at 550 F were estimated by ratioing the room temperature CMTR values to the same ratio found in the ASME Code [25] for the decrease in strength between room temperature and 550°F. Furthermore, it has been shown that thermal aging leads to an increase in yield and ultimate tensile strength, and a slight decrease in ductility [21], which results in an increased flow stress. For CF8M cast stainless steels, this increase in flow stress at room temperature and 550°F is 19% and 24%, respectively, as shown in Figures 4-11 and 4-12. To accurately determine the blunting line for  $J_{Ic}$  determination, the flow stress values were, therefore, increased accordingly.

The lower bound value of  $K_{Ic}$  used for linear elastic fracture mechanics analysis is determined from  $J_{Ic}$  using the relationship:



$$K_{Ic} = \sqrt{\frac{E J_{Ic}}{(1 - \nu^2)}} \quad (4-18)$$

where E is the elastic modulus (equals  $25.5 \times 10^6$  psi [2], and  $\nu$  is Poisson's ratio (equals 0.3).

A summary of the results presented in Tables 4-1 and 4-2 shows that for the CF8M pump casings at Davis-Besse, the range of  $J_{Ic}$  (including long-term aging effects (embrittlement)) is 690-2302 in-lb/in<sup>2</sup>. This minimum value of 690 in-lb/in<sup>2</sup> translates into a  $K_{Ic}$  value of 139 ksi√in at the operating temperature of 557°F.

#### ***4.1.2 Fracture Toughness of Pump Casing Weldments***

As indicated earlier, the fabrication records indicate that the pump casing weldments were made using flux welding, either by submerged arc welding (SAW) or shielded metal arc welding (SMAW). Extensive work done in References 26 and 27 on the toughness of austenitic stainless steel weldments has shown that the toughness for SAW and SMAW weldments in the unaged condition is lower than for the base material. On the other hand, tungsten inert gas (TIG or GTAW) weldments have toughness more typical of the base metal. The lower toughness of SAW and SMAW weldments is due to nonmetallic inclusions in the weld metal that result from the flux welding process. Because of the low initial values, the fracture toughness of SMAW and SAW weld metals are only slightly affected by long-term aging. Limited data from Reference 26 suggests that  $J_{Ic}$  values of 1168 and 973 in-lb/in<sup>2</sup> may be used for SMAW and SAW weldment fracture assessments, respectively, in the as-welded condition. Corresponding values for solution-annealed weldments are 963 and 1260 in-lb/in<sup>2</sup>. Values of 990 and 650 in-lb/in<sup>2</sup> are suggested in Reference 28 for SMAW and SAW, respectively, based on the work done in Reference 27. These values are very comparable to the lowest fracture toughness calculated for the base metal considering embrittlement. Hence, the lowest fracture toughness for the base metal calculated in Table 4-1 is used for this evaluation. The methodology used to determine the lower bound fracture toughness for the base metal was also employed for the weld metal and the results presented in Table 4-2. As can be seen from this table, the saturation fracture toughness

values for the weld metals far exceed that for the base metal, justifying the use of the lower bound base metal toughness for this evaluation.

## **4.2 Stress Analysis Results**

In performing the evaluations, the possibility of using previous stress analyses in the existing Stress Report [4] for the pump casing was explored. It was observed that detailed through-wall stress information was not available to perform flaw evaluation of critical locations for all load cases. As such, a three dimensional finite element model was developed for the purpose of determining the operating stresses in the pump casing.

The finite element model of the pump casing was developed using the ANSYS computer software [29]. The dimensions used for the model obtained from References 4, 6, 30 and 31 are shown in Figure 4-13 through 4-15. The finite element model is shown in Figure 4-16 and 4-17. It was generated using isoparametric finite elements for the casing. Three stress cases were run using this model to determine the stress response.

### **4.2.1 Pressure**

A pressure of 2250 psig was applied to the inside surface of the model. This pressure corresponds to the operating pressure. The resulting stress intensity distribution for the pressure case is shown in Figure 4-18. Summary of the axial and hoop pressure stresses for the thirteen critical paths of the model are presented in Table 4-3.

### **4.2.2 Heatup Thermal Transient**

The definition of the heatup transient for Davis-Besse is provided in Reference 4. The transient involves ramping the inside temperature from 70°F to 557°F in 4.87 hours (100°F per hour). In the thermal analysis, the outside surface was initially kept at 70°F. A film coefficient of 1000 Btu/hr-ft<sup>2</sup>-°F was used on the inside surface consistent with the reactor coolant flow inside the pump. The outside surface was assumed to be insulated and therefore a conservative heat



transfer coefficient of 1 Btu/hr-ft<sup>2</sup>-°F was used. The temperature distribution at the most critical time during heatup is shown in Figure 4-19. The resulting temperature distribution was used to perform a stress analysis. The stress intensity plots at the most critical time is shown in Figure 4-20. Hoop and axial stresses for the thirteen critical paths of the model are shown in Table 4-3.

#### **4.2.3 *Cooldown Thermal Transient***

For the cooldown transient, the definition provided in Reference 4 was used. It involves multiple ramps of RCS temperature from 557°F to 140°F. The first phase involves ramping the inside from 557°F to 280°F in 6 hours (46.17°F per hour). The final phase is a ramp from 280°F to 140°F in 8 hours (17.5°F per hour). Figure 4-21 shows the temperature distribution at the most critical time. The resulting stress distribution is shown in Figure 4-22. Summary of the hoop and axial stresses for the cooldown transient are presented in Table 4-3.

#### **4.2.4 *Residual Stresses***

In addition to the applied stresses, weld residual stresses need to be addressed in this evaluation. In the evaluation of pressure vessels per ASME Code, Appendix G, residual stresses are not considered, because the vessel is postweld heat treated after welding to minimize the effect of residual stresses. Similarly, since the pump casings were solution heat treated subsequent to welding and weld repairs, residual stresses are expected to be minimal and are, therefore, not considered in this evaluation.

### **4.3 *Review of Operating History of the Pumps***

Davis-Besse has been in commercial operation since November 1, 1977. The plant has undergone fifty (50) heatups and forty-nine (49) cooldowns as of this date. At this point in time, these numbers are well below the expected number of heatup/cooldown cycles, based upon the design number of heatup/cooldown cycles (240 for a 40-year plant life).



The four RCPs at Davis-Besse have experienced essentially the same individual operating histories. The normal operating pressure and temperature for the RCPs are 2,250 psig and 557°F, respectively.

#### **4.4 Selection of Locations for Postulating**

The following selection criteria was used for the determination of locations for postulating flaws:

- Areas of low fracture toughness
- Highly stressed locations
- Areas of geometric discontinuity
- Locations where flaws have been identified in previous inspections.

Since the lower bound fracture toughness is used in the evaluation and no flaws have been found in previous inspections, the most highly stressed locations (which correspond to areas of geometric discontinuities) were chosen as the location for potential flaws. Thirteen highly stressed locations shown in Figures 4-24 and 4-25 are used in the evaluation.

#### **4.5 Postulated Flaw**

As required by the Code Case, the postulated flaw is a quarter-thickness semi-elliptical flaw with length six times the depth. The thickness of the pump casing at the thirteen critical locations and the associated flaw sizes are shown in Table 4-4.

#### **4.6 Determination of Stability of Postulated Flaw**

To determine the stability of the postulated flaw, fracture mechanics evaluations are performed at the critical weld location to address the following:



- 1) Determination of applied stress intensity factors
- 2) Allowable stress intensity factor
- 3) Fatigue crack growth
- 4) Stress corrosion crack growth.

#### **4.6.1 Determination of Applied Stress Intensity Factors**

Even though austenitic stainless steels have been shown to be relatively ductile materials, linear elastic fracture mechanics (LEFM) techniques were conservatively used in lieu of elastic-plastic fracture mechanics (EPFM) techniques.

The stress intensity factors ( $K_I$ ) associated with the applied stresses were conservatively determined using the flat plate model of ASME Code, Section XI, Appendix A [32]. The expression for  $K_I$  is given by:

$$K_I = \sigma_m M_m \sqrt{\pi} \sqrt{a/Q} + \sigma_b M_b \sqrt{\pi} \sqrt{a/Q}$$

where:

- $\sigma_m, \sigma_b$  = membrane and bending stresses, respectively
- $a$  = minor half-diameter of embedded flaw; flaw depth for surface flaw
- $Q$  = flaw shape parameter
- $M_m$  = correction factor for membrane stress
- $M_b$  = correction factor for bending stress

The above model is contained in the library of Structural Integrity Associates' computer software **pc-CRACK** [33]. This software was, therefore, used to determine the stress intensity factors at the various locations, using the stress information contained in Table 4-3. In order to use **pc-CRACK**, the through-thickness stresses are curve fit to a third degree polynomial to determine the membrane and the bending components.



#### 4.6.2 Allowable Stress Intensity Factor

Stress intensity factors, for comparison to an allowable value, were calculated consistent with the safety factors provided in Appendix G of Section XI of the ASME Code. Paragraph G-2222 requires a safety factor of 2.0 on primary stresses and a safety factor of 1.0 on secondary stresses for Service Levels A and B.

The evaluation is performed for normal operating and upset conditions (Levels A and B) since no specific requirements are stipulated for emergency and faulted conditions (Levels C and D) in Appendix G of ASME Section XI. The terms whose sum must be less than the allowable reference stress intensity factor ( $K_{IR}$ ) for Levels A and B operating conditions (Service Levels A and B) are:

- 1)  $2K_{Im}$  for primary membrane stress
- 2)  $2K_{Ib}$  for primary bending stress
- 3)  $K_{Im}$  for secondary membrane stress
- 4)  $K_{Ib}$  for secondary bending stress.

Table 4-5 presents the stress intensity factors with the appropriate safety factors at the critical location for normal/upset and emergency/faulted conditions, and their comparison to the allowable  $K_{IR}$  value of  $139.0 \text{ ksi}\sqrt{\text{in}}$ . In this evaluation, the operating pressure of 2250 psig was used. The stress intensity factors associated with this pressure were conservatively added to either the heatup or cooldown transient stress intensity factor to determine the final value to compare with the allowables. The analysis was performed using the postulated quarter-thickness flaw depth. It can be seen that the stress intensity factors are below the allowable values both in the axial and circumferential directions.



#### 4.6.3 Fatigue Crack Growth

Fatigue crack growth analyses were performed to assure that crack growth for a small initial assumed flaw will not grow beyond the quarter-thickness flaw considered in the Code Case. Since previous inspections have not identified any flaws in the pump casing welds, an initial flaw corresponding to the acceptance standards of ASME Code, Section XI, Subarticle IWB-3500 was assumed. For the pump casing welds, this corresponds to an initial depth of 10% of wall thickness. The flaw was conservatively postulated on the inside surface of the pump casing, which would require consideration of the PWR water environment at 550 F. A fatigue crack growth law for a water environment is not currently in the ASME Code Section XI; however, a crack growth law for austenitic stainless steel in an air environment is provided in ASME Code, Section XI, Appendix C [32]. Per the recommendation of ASME Code, Section XI Task Group for Piping Flaw Evaluation [34], a factor of 2 was applied to the air environment law to account for the PWR water environment. The ASME Code, Section XI fatigue crack growth law for air is given as:

$$\frac{da}{dN} = C_o (\Delta K_I)^n$$

where  $n$  equals 3.3, and

$$C_o = C(S)$$

where  $C$  is a scaling parameter to account for temperature, and is given by:

$$C = 10^{[-10.009 = 8.12 \times 10^{-4} T - 1.13 \times 10^{-6} T^2 + 1.02 \times 10^{-9} T^3]}$$

$T$  is the metal temperature in °F ( $T \leq 800$  F).  $S$  is a scaling parameter to account for the  $R$  ratio ( $K_{min}/K_{max}$ ), and is given by:

$$S = 1.0 \quad \text{when } R \leq 0$$





$$\begin{aligned}
 &= 1.0 + 1.8R && \text{when } 0 < R \leq 0.79 \\
 &= -43.35 + 57.97R && \text{when } 0.79 < R \leq 1.0
 \end{aligned}$$

At a temperature of 550°F, and for  $R \leq 0$  as in this case,  $C_o$  was calculated as  $1.84 \times 10^{-10}$  for an air environment. A value of  $C_o$  of  $3.68 \times 10^{-10}$  was, therefore, used for the PWR water environment to determine crack growth for flaws on the inside surface.

Fatigue crack growth analysis requires cyclic loading information. Cyclic information for Davis-Besse RCP casing design transients provided in Reference 4 were reviewed. The only significant transients in this table are heatup/cooldowns, loss of secondary pressure, hydrotest and leak test, since these are associated with very high pressure and temperature changes. The total number of cycles associated with these transients is 240. All other transients are judged to contribute insignificantly to crack growth. The stresses for the normal/upset load combination are the same as for the test load combination, and, therefore, the analysis was performed using the normal/upset stresses. The analysis was performed using **pc-CRACK**.

The results from the fatigue crack growth analysis are summarized in Table 4-6 for the most highly stressed locations (Paths 5, 10, 11, 12 and 13). Crack growth results for the most critical location (Path 13) is also presented in Figure 4-23. The results show that fatigue crack growth is relatively small during the 40-year plant life (240 cycles). In fact, after 2000 cycles, the initial 10% through-wall flaw at the most critical location (axial flaw at Path No. 13) has grown to only 15%, indicating that the quarter-thickness flaw bounds any flaw that may be identified during service. Considering the fact that Davis-Besse has gone through 50/49 heatups/ cooldowns, and 9 scheduled hydrostatic/system leak tests in twenty-three years, it is predicted that the quarter-thickness flaw will not be reached during the lifetime of the plant.

#### 4.6.4 Stress Corrosion Crack Growth

Stress corrosion cracking (SCC) in pressurized water reactor plants is not generally of concern, since the environment is not usually conducive to SCC due to its reducing nature. Moreover, stainless steel castings have been shown to have superior resistance to SCC when compared to

wrought products. A wrought material consists of a single phase austenite ( $\gamma$ ). When such a material is welded, the thermal cycles cause chromium carbides to be precipitated from solution and deposited at austenite-austenite ( $\gamma - \gamma$ ) grain boundaries. The diffusion of chromium from the austenite matrix results in a chromium-depleted zone at the grain boundary, resulting in sensitization. On the other hand, when a stainless steel casting (a two-phase duplex microstructure) is exposed to the same thermal cycle, carbon and chromium also combine to form grain boundary carbides; however, these carbides form exclusively at the austenite-ferrite ( $\gamma$ - $\delta$ ) boundaries, with the majority of the chromium diffusing from the delta ferrite side of the boundary (diffusion of chromium in the ferrite is approximately 1000 times faster than that in austenite at a temperature of 1100 F). Thus, the chromium content of the austenite is not reduced significantly, and corrosion resistance, even near the  $\gamma$ - $\delta$  grain boundary, is maintained. Crack growth due to SCC will, therefore, not be considered in this evaluation.

#### **4.7 Effect of Thermal Embrittlement and Other Degradation Mechanisms that May Degrade Properties of the Pump Casing**

Structural material degradation mechanisms for various components in light water reactors have been discussed extensively in Reference 35. Of all the degradation mechanisms addressed in the Reference 35 EPRI report, only thermal and irradiation embrittlement could potentially degrade the fracture toughness properties of the cast stainless steel pump casings. Thermal embrittlement effects have been included in the consideration of crack growth and fracture toughness ( $K_{IR}$ ) properties in this study. Irradiation embrittlement is not of concern since the RCPs are far removed from the reactor core.



Table 4-1

Determination of Lower Bound Fracture Toughness of Davis-Besse Pump Casings  
Considering Thermal Embrittlement

	P1A1		P1A2		P1B1		P1B1	
	S/N: 701-N-0240		S/N: 701-N-0242		S/N: 701-N-0243		S/N: 701-N-0241	
	Hub	Scroll	Hub	Scroll	Hub	Scroll	Hub	Scroll
	S/N: 6795 Ht#: 6573	S/N: 6778 Ht#: 6536	S/N: 6777 Ht#: 6527	S/N: 6774 Ht#: 6513	S/N: 6775 Ht#: 6518	S/N: 6794 Ht#: 6555	S/N: 6793 Ht#: 6554	S/N: 6774 Ht#: 6513
<b>Mechanical Properties</b>								
Yield Strength (psi)	33000	34500	37000	36000	32000	36000	33500	33750
Ultimate Tensile Str. (psi)	72500	76500	73750	71250	71500	75000	71250	75250
Elongation (%)	51	49.5	59	46	55	48.5	50	60
<b>Chemical Properties</b>								
Cr	18.6	18.5	18.8	18.8	18.6	18.6	18.3	18.6
Si	0.87	0.93	0.81	0.78	0.72	0.88	0.74	0.74
Mo	2.15	2.16	2.18	2.14	2.19	2.18	2.1	2.15
Ni	9.3	9.4	9.4	9.5	9.6	9.5	9.1	9.42
C	0.06	0.06	0.04	0.02	0.03	0.04	0.05	0.04
Mn	0.98	1.04	0.92	0.8	0.98	1.03	0.98	0.98
N (*assumed)	0.044	0.057	0.04*	0.047	0.047	0.05	0.052	0.051
Cr <sub>eq</sub>	16.6	16.6	16.8	16.8	16.6	16.7	16.2	16.6
Ni <sub>eq</sub>	14.4	14.8	14.0	13.7	14.1	14.3	14.2	14.2
Ferrite ( $\delta_c$ )	10.6	8.8	14.1	15.5	12.4	11.6	10.3	11.5
$\Phi$	20.4	18.9	19.6	14.8	15.5	18.2	17.0	17.3
Cv <sub>sat</sub> (J/cm <sup>2</sup> ) [Polynomial]	127.7	122.5	140.5	174.1	187.2	144.7	188.8	171.7
Cv <sub>sat</sub> (J/cm <sup>2</sup> ) [ $\Phi$ ]	104.0	119.2	112.4	180.7	166.9	127.6	143.2	139.3
Minimum Cv <sub>sat</sub> (J/cm <sup>2</sup> )	104.0	119.2	112.4	174.1	166.9	127.6	143.2	139.3
C (J-R Curve Constant)	5739.2	6135.7	5961.9	7386.1	7234.9	6342.3	6712.5	6621.9
N (J-R Curve Exponent)	0.345	0.348	0.347	0.358	0.357	0.350	0.353	0.352
J <sub>1c</sub> (in-lb/in <sup>2</sup> )	1429.2	1532.3	1486.9	1867.7	1826.3	1586.6	1684.9	1660.7
K <sub>1c</sub> (ksi-in <sup>1/2</sup> )	200.1	207.2	204.1	228.8	226.2	210.9	217.3	215.7



Table 4-2

Determination of Lower Bound Fracture Toughness of Davis-Besse Pump Casings  
Welds Considering Thermal Embrittlement

	ARCOSARC SS-3, 3/32 Lot#:1942RC (First of Run) (ARCOS)	ARCOSARC SS-3, 3/32 Lot#:1942RC (Middle of Run) (ARCOS)	ARCOSARC SS-3, 3/32 Lot#:1942RC (End of Run) (ARCOS)	ARCOSARC SS-3, 3/32 Lot#:1F09B (First of Run) (ARCOS)	ARCOSARC SS-3, 3/32 Lot#:1F09B (Middle of Run) (ARCOS)	ARCOSARC SS-3, 3/32 Lot#:1F09B (End of Run) (ARCOS)
<b>Properties Chemical</b>						
Cr	20.54	19.9	20.26	20.22	19.29	19.27
Si	0.41	0.63	0.64	0.28	0.41	0.51
Mo	2.5	2.43	2.47	2.51	2.49	2.48
Ni	10.73	10.43	10.59	10.22	10.34	10.32
C	0.049	0.059	0.055	0.056	0.056	0.053
Mn	0.89	1.27	1.28	1.44	1.13	1.15
N (assumed)	0.04	0.04	0.04	0.04	0.04	0.04
Cr <sub>eq</sub>	18.8	18.2	18.6	18.4	17.5	17.5
Ni <sub>eq</sub>	15.5	15.5	15.6	15.2	15.3	15.2
Ferrite ( $\delta_c$ )	14.4	11.8	13.3	14.3	10.1	10.5
$\Phi$	27.1	26.9	29.5	29.4	20.5	20.9
Cv <sub>sat</sub> (J/cm <sup>2</sup> ) [Polynomial]	68.0	72.7	59.9	82.9	121.7	114.0
Cv <sub>sat</sub> (J/cm <sup>2</sup> ) [ $\Phi$ ]	36.7	37.2	31.6	31.8	64.9	62.2
Minimum Cv <sub>sat</sub> (J/cm <sup>2</sup> )	36.7	37.2	31.6	31.8	64.9	62.2
C (J-R Curve Constant)	3445.5	3467.3	3203.0	3209.3	4555.1	4462.0
N (J-R Curve Exponent)	0.319	0.320	0.316	0.316	0.333	0.332
J <sub>1c</sub> (in-lb/in <sup>2</sup> )	863.0	868.2	805.7	807.1	1130.9	1108.1
K <sub>1c</sub> (ksi-in <sup>1/2</sup> )	155.5	156.0	150.3	150.4	178.0	176.2

Table 4-2 (continued)

Determination of Lower Bound Fracture Toughness of Davis-Besse Pump Casings  
Welds Considering Thermal Embrittlement

	ARCOSARC SS-3, 3/32 Lot#:1B13L42C (First of Run) (ARCOS)	ARCOSARC SS-3, 3/32 Lot#:1B13L42C (Middle of Run) (ARCOS)	ARCOSARC SS-3, 3/32 Lot#:1B13L42C (End of Run) (ARCOS)	ARCOSARC SS-3, 3/32 Lot#:1B13L (First of Run) (ARCOS)	ARCOSARC SS-3, 3/32 Lot#:1B13L (Middle of Run) (ARCOS)	ARCOSARC SS-3/32 Lot#:1B13L (End of Run) (ARCOS)
<b>Properties Chemical</b>						
Cr	19.59	19.53	19.21	20.16	19.55	19.71
Si	0.51	0.65	0.57	0.59	0.68	0.68
Mo	2.93	2.86	3	2.82	2.91	2.88
Ni	10.82	10.71	10.77	10.52	10.76	10.99
C	0.046	0.05	0.045	0.051	0.054	0.049
Mn	1.19	1.2	1.14	1.34	1.5	1.35
N (assumed)	0.04	0.04	0.04	0.04	0.04	0.04
Cr <sub>eq</sub>	18.4	18.3	18.1	18.9	18.4	18.5
Ni <sub>eq</sub>	15.6	15.6	15.5	15.4	15.7	15.8
Ferrite ( $\delta_c$ )	12.5	12.2	11.8	15.6	11.8	11.8
$\Phi$	24.3	25.4	22.4	32.3	27.6	26.1
Cv <sub>sat</sub> (J/cm <sup>2</sup> ) [Polynomial]	69.1	62.8	74.1	48.2	56.0	56.4
Cv <sub>sat</sub> (J/cm <sup>2</sup> ) [ $\Phi$ ]	45.5	41.5	53.9	27.1	35.6	39.7
Minimum Cv <sub>sat</sub> (J/cm <sup>2</sup> )	45.5	41.5	53.9	27.1	35.6	39.7
C (J-R Curve Constant)	3826.6	3657.3	4156.1	2971.1	3393.5	3577.1
N (J-R Curve Exponent)	0.325	0.322	0.329	0.312	0.318	0.321
J <sub>1c</sub> (in-lb/in <sup>2</sup> )	953.9	913.4	1033.4	751.3	850.7	894.3
K <sub>1c</sub> (ksi-in <sup>1/2</sup> )	163.5	160.0	170.2	145.1	154.4	158.3



Table 4-2 (continued)

Determination of Lower Bound Fracture Toughness of Davis-Besse Pump Casings  
Welds Considering Thermal Embrittlement

	ARCOSARC Chromend 316 Lot#:0K9B (ARCOS)	ARCOSARC Chromend 316 Lot#:0F21B Mix31A . (ARCOS)	ARCOSARC Chromend E316-15 Lot#:1D11A Mixes 9 and 31 (ARCOS)	ARCOSARC Chromend 316-15 Lot#:OH10B- 18 (ARCOS)	ARCOSARC Stainend 3/16 Lot#:9K26B (ARCOS)	ARCOS Lot#:1942RC (GE)
<b>Properties Chemical</b>						
Cr	20.33	19.33	19.73	20.63	19.91	20.5
Si	0.23	0.29	0.17	0.31	0.33	0.6
Mo	2.02	2.12	2.08	2.22	2.06	2.43
Ni	10.53	10.6	11.34	11.32	10.93	10.1
C	0.038	0.061	0.034	0.029	0.04	0.06
Mn	1.57	1.43	1.51	1.51	1.73	1.24
N (assumed)	0.04	0.04	0.04	0.04	0.04	0.04
Cr <sub>eq</sub>	17.9	17.0	17.3	18.5	17.6	18.7
Ni <sub>eq</sub>	15.1	15.7	15.8	15.7	15.6	15.2
Ferrite ( $\delta_c$ )	12.7	7.0	7.6	12.3	9.3	16.2
$\Phi$	20.8	16.3	12.8	19.1	17.5	35.1
Cv <sub>sat</sub> (J/cm <sup>2</sup> ) [Polynomial]	159.4	189.4	244.1	119.7	176.0	51.7
Cv <sub>sat</sub> (J/cm <sup>2</sup> ) [ $\Phi$ ]	62.7	107.5	182.3	75.3	91.6	24.0
Minimum Cv <sub>sat</sub> (J/cm <sup>2</sup> )	62.7	107.5	182.3	75.3	91.6	24.0
C (J-R Curve Constant)	4478.3	5831.9	7555.3	4899.4	5392.4	2794.1
N (J-R Curve Exponent)	0.332	0.346	0.359	0.337	0.342	0.309
J <sub>1c</sub> (in-lb/in <sup>2</sup> )	1112.0	1453.2	1914.4	1216.3	1340.5	710.0
K <sub>1c</sub> (ksi-in <sup>1/2</sup> )	176.5	201.8	231.6	184.6	193.8	141.1



Table 4-2 (continued)

Determination of Lower Bound Fracture Toughness of Davis-Besse Pump Casings  
Welds Considering Thermal Embrittlement

	ARCOS Lot#: 1F09B (GE)	ARCOS Lot#: 1B13L42C (GE)	ARCOS Lot#: 1B13L (GE)	ARCOS Lot#: 0F21B (GE)	ARCOS Lot#: 1D11A (GE)	ARCOS Lot#: 0H10B (GE)
<b>Properties Chemical</b>						
Cr	20.4	19.6	20.2	19.2	18.9	20.8
Si	0.51	0.69	0.72	0.36	0.25	0.41
Mo	2.57	2.85	2.83	1.96	2.1	2.26
Ni	10.1	10.4	10.2	10.3	11	11.1
C	0.06	0.06	0.05	0.05	0.04	0.04
Mn	1.08	1.43	1.41	1.38	1.6	1.5
N (assumed)	0.04	0.04	0.04	0.04	0.04	0.04
Cr <sub>eq</sub>	18.8	18.4	19.0	16.8	16.6	18.7
Ni <sub>eq</sub>	15.2	15.5	15.1	15.2	15.6	15.7
Ferrite ( $\delta_c$ )	16.4	12.8	18.3	8.0	5.9	13.2
$\Phi$	34.1	30.4	36.7	15.4	11.0	25.0
Cv <sub>sat</sub> (J/cm <sup>2</sup> ) [Polynomial]	52.3	52.5	38.9	235.0	308.9	84.5
Cv <sub>sat</sub> (J/cm <sup>2</sup> ) [ $\Phi$ ]	25.0	29.9	22.5	122.4	255.8	43.0
Minimum Cv <sub>sat</sub> (J/cm <sup>2</sup> )	25.0	29.9	22.5	122.4	255.8	43.0
C (J-R Curve Constant)	2852.5	3117.2	2707.3	6214.4	8919.1	3720.2
N (J-R Curve Exponent)	0.310	0.314	0.307	0.349	0.367	0.323
J <sub>1c</sub> (in-lb/in <sup>2</sup> )	723.6	785.6	689.8	1552.8	2302.3	928.3
K <sub>1c</sub> (ksi-in <sup>1/2</sup> )	142.4	148.4	139.0	208.6	254.0	161.3



Table 4-2 (continued)

Determination of Lower Bound Fracture Toughness of Davis-Besse Pump Casings  
Welds Considering Thermal Embrittlement

	ARCOS Lot#: 9K26B (GE)	5/32; Stoody; E316L-16 Lot#:T04630 (Stoody)	3/16; Stoody; E316ELC-16 Lot#:T04595 (Stoody)	3/16; Stoody; E316L-16 Lot#:T05005 (Stoody)	3/16; Stoody; E316ELC-16 Lot#:T04365 (Stoody)	Stoody; Lot#:T04630 (GE)
<b>Properties Chemical</b>						
Cr	19.9	19.04	18.91	19.05	18.56	19.4
Si	0.28	0.42	0.42	0.37	0.42	0.37
Mo	2	2.38	2.4	2.23	2.54	2.4
Ni	10.6	11.86	11.78	11.75	11.33	11.8
C	0.04	0.034	0.034	0.035	0.032	0.06
Mn	1.9	1.53	1.36	1.57	1.47	1.3
N (assumed)	0.04	0.04	0.04	0.04	0.04	0.04
Cr <sub>eq</sub>	17.5	17.1	17.0	16.9	16.8	17.5
Ni <sub>eq</sub>	15.3	16.3	16.3	16.3	15.8	16.9
Ferrite ( $\delta_c$ )	10.2	5.5	5.4	5.2	6.3	5.0
$\Phi$	18.6	10.4	10.0	9.9	10.6	13.7
Cv <sub>sat</sub> (J/cm <sup>2</sup> ) [Polynomial]	192.4	204.8	213.2	243.4	221.2	139.1
Cv <sub>sat</sub> (J/cm <sup>2</sup> ) [ $\Phi$ ]	79.5	285.1	309.4	313.9	274.7	158.6
Minimum Cv <sub>sat</sub> (J/cm <sup>2</sup> )	79.5	204.8	213.2	243.4	221.2	139.1
C (J-R Curve Constant)	5031.5	7998.3	8157.0	8704.5	8305.9	6617.7
N (J-R Curve Exponent)	0.338	0.362	0.363	0.366	0.364	0.352
J <sub>1c</sub> (in-lb/in <sup>2</sup> )	1249.4	2038.2	2083.1	2239.9	2125.3	1659.6
K <sub>1c</sub> (ksi-in <sup>1/2</sup> )	187.1	239.0	241.6	250.5	244.0	215.7





Table 4-2 (concluded)

Determination of Lower Bound Fracture Toughness of Davis-Besse Pump Casings  
Welds Considering Thermal Embrittlement

	Stoody; Lot#:T04595 (GE)	Stoody; Lot#:T05005 (GE)	Stoody; Lot#:T04365 (GE)
<b>Properties Chemical</b>			
Cr	19.7	19.2	18.9
Si	0.35	0.28	0.37
Mo	2.4	2.42	2.54
Ni	11.9	11.4	11.3
C	0.03	0.04	0.03
Mn	1.3	1.27	1.5
N (assumed)	0.04	0.04	0.04
Cr <sub>eq</sub>	17.8	17.3	17.2
Ni <sub>eq</sub>	16.3	16.0	15.7
Ferrite ( $\delta_c$ )	7.4	6.8	7.5
$\Phi$	12.6	12.7	12.0
Cv <sub>sat</sub> (J/cm <sup>2</sup> ) [Polynomial]	162.3	195.3	200.1
Cv <sub>sat</sub> (J/cm <sup>2</sup> ) [ $\Phi$ ]	190.8	185.9	212.8
Minimum Cv <sub>sat</sub> (J/cm <sup>2</sup> )	162.3	185.9	200.1
C (J-R Curve Constant)	7135.6	7627.8	7907.1
N (J-R Curve Exponent)	0.356	0.359	0.361
J <sub>1c</sub> (in-lb/in <sup>2</sup> )	1799.3	1934.6	2012.6
K <sub>1c</sub> (ksi-in <sup>1/2</sup> )	224.5	232.8	237.5

The range of J<sub>1c</sub> (including long-term effects, i.e. embrittlement) for the weldments is 690 to 2302 in-lb/in<sup>2</sup>. The resulting K<sub>1c</sub> for a J<sub>1c</sub> of 690 is 139 ksi-in<sup>1/2</sup> at an operating temperature of 550°F.

Table 4-3

## Summary of Stresses

Path Number	Axial Stress (ksi)					
	Pressure		Heatup		Cooldown	
	Membrane	Bending	Membrane	Bending	Membrane	Bending
1	2.473	0.733	-3.577	13.360	1.105	2.743
2	3.080	1.102	-5.816	8.338	2.156	1.492
3	4.521	0.871	-8.167	5.112	3.005	0.775
4	4.947	1.299	-14.550	2.422	5.651	0.068
5	5.244	0.815	-12.450	3.603	4.692	0.657
6	4.475	0.364	0.672	23.870	0.154	8.024
7	4.876	0.327	-5.126	18.740	2.607	6.087
8	5.950	0.482	-10.290	15.670	4.757	4.972
9	6.215	0.989	-12.410	17.810	5.701	5.568
10	4.055	1.812	-1.074	22.960	0.665	6.999
11	4.918	0.544	-5.368	17.880	2.164	5.318
12	6.473	0.722	-7.807	13.820	3.178	3.968
13	6.546	2.443	-8.542	14.075	3.593	3.541

Path Number	Hoop Stress (ksi)					
	Pressure		Heatup		Cooldown	
	Membrane	Bending	Membrane	Bending	Membrane	Bending
1	6.032	1.813	0.289	12.130	-0.093	2.276
2	7.936	3.884	0.507	8.504	-0.042	2.124
3	9.521	2.820	0.761	6.219	-0.157	1.705
4	9.383	4.840	1.119	1.798	-0.156	0.694
5	7.456	0.183	-5.448	4.893	3.509	1.152
6	6.119	0.033	-0.542	27.230	-0.313	8.574
7	6.205	2.767	-0.166	23.940	-0.448	7.480
8	7.534	2.459	-0.324	22.810	-0.288	7.013
9	6.883	4.022	1.083	31.440	-0.947	9.747
10	7.043	1.652	1.066	27.690	-0.615	8.363
11	7.256	4.579	1.388	28.570	-0.874	8.766
12	7.928	3.586	-0.436	25.630	-0.168	7.809
13	6.731	8.055	-0.594	29.390	-0.182	7.857



**Table 4-4**  
**Thickness and Flaw Dimensions at Postulated Flaw Locations**

Path No.	Wall Thickness (in)	Flaw Depth (in)	Flaw Length (in)
1	5.00	1.250	7.500
2	3.70	0.925	5.550
3	2.50	0.625	3.750
4	2.20	0.550	3.300
5	2.10	0.525	3.150
6	5.00	1.250	7.500
7	3.70	0.925	5.550
8	2.50	0.625	3.750
9	2.20	0.550	3.300
10	5.00	1.250	7.500
11	3.70	0.925	5.550
12	2.50	0.625	3.750
13	2.20	0.550	3.300

Table 4-5  
Comparison of Calculated and Allowable Stress Intensity Factors

Pressure + Heatup Axial Stress Case						
Path Number	Stress Intensity Factor (ksi $\sqrt{\text{in}}$ )					
	2 x Pressure		Heatup		Total	Allowable
	Membrane	Bending	Membrane	Bending		
1	10.786	2.118	-7.801	19.302	24.406	139.0
2	11.556	2.739	-10.911	10.363	13.747	139.0
3	13.944	1.780	-12.594	5.222	8.351	139.0
4	14.313	2.490	-21.048	2.321	-1.924	139.0
5	14.823	1.526	-17.596	3.374	2.127	139.0
6	19.519	1.052	1.465	34.487	56.523	139.0
7	18.295	0.813	-9.616	23.291	32.782	139.0
8	18.351	0.985	-15.868	16.009	19.476	139.0
9	17.981	1.896	-17.952	17.068	18.993	139.0
10	17.687	5.236	-2.342	33.172	53.752	139.0
11	18.452	1.352	-10.070	22.222	31.956	139.0
12	19.964	1.475	-12.039	14.119	23.519	139.0
13	18.939	4.683	-12.357	13.489	24.754	139.0

Pressure + Heatup Hoop Stress Case						
Path Number	Stress Intensity Factor (ksi $\sqrt{\text{in}}$ )					
	2 x Pressure		Heatup		Total	Allowable
	Membrane	Bending	Membrane	Bending		
1	26.310	5.239	0.630	17.525	49.704	139.0
2	29.776	9.654	0.952	10.569	50.952	139.0
3	29.364	5.762	1.173	6.353	42.653	139.0
4	27.147	9.277	1.619	1.723	39.766	139.0
5	21.076	0.343	-7.700	4.581	18.300	139.0
6	26.689	0.095	-1.182	39.341	64.944	139.0
7	23.281	6.878	-0.311	29.754	59.602	139.0
8	23.236	5.024	-0.500	23.303	51.064	139.0
9	19.914	7.709	1.567	30.131	59.321	139.0
10	30.719	4.774	2.325	40.006	77.824	139.0
11	27.225	11.382	2.604	35.508	76.719	139.0
12	24.451	7.327	-0.673	26.184	57.290	139.0
13	19.474	15.439	-0.859	28.166	62.221	139.0

Table 4-5

Comparison of Calculated and Allowable Stress Intensity Factors  
(Continued)

Pressure + Cooldown Axial Stress Case						
Path Number	Stress Intensity Factor (ksi $\sqrt{\text{in}}$ )					
	2 x Pressure		Cooldown		Total	Allowable
	Membrane	Bending	Membrane	Bending		
1	10.786	2.118	2.410	3.963	19.277	139.0
2	11.556	2.739	4.045	1.854	20.194	139.0
3	13.944	1.780	4.634	0.792	21.149	139.0
4	14.313	2.490	8.175	0.065	25.042	139.0
5	14.823	1.526	6.631	0.615	23.596	139.0
6	19.519	1.052	0.336	11.593	32.500	139.0
7	18.295	0.813	4.891	7.565	31.564	139.0
8	18.351	0.985	7.336	5.079	31.751	139.0
9	17.981	1.896	8.247	5.336	33.460	139.0
10	17.687	5.236	1.451	10.112	34.485	139.0
11	18.452	1.352	4.060	6.609	30.474	139.0
12	19.964	1.475	4.901	4.054	30.394	139.0
13	18.939	4.683	5.198	3.394	32.213	139.0

Pressure + Cooldown Hoop Stress Case						
Path Number	Stress Intensity Factor (ksi $\sqrt{\text{in}}$ )					
	2 x Pressure		Cooldown		Total	Allowable
	Membrane	Bending	Membrane	Bending		
1	26.310	5.239	-0.203	3.288	34.634	139.0
2	29.776	9.654	-0.079	2.640	42.104	139.0
3	29.364	5.762	-0.242	1.742	36.626	139.0
4	27.147	9.277	-0.226	0.665	36.863	139.0
5	21.076	0.343	4.959	1.079	27.457	139.0
6	26.689	0.095	-0.683	12.388	38.489	139.0
7	23.281	6.878	-0.840	9.297	38.615	139.0
8	23.236	5.024	-0.444	7.165	34.981	139.0
9	19.914	7.709	-1.370	9.341	35.594	139.0
10	30.719	4.774	-1.340	12.083	46.235	139.0
11	27.225	11.382	-1.640	10.895	47.862	139.0
12	24.451	7.327	-0.258	7.978	39.497	139.0
13	19.474	15.439	-0.263	7.530	42.181	139.0



Table 4-6  
Fatigue Crack Growth Evaluation Results

Path No.	Axial Flaw				Circumferential Flaw			
	Initial Flaw Size		Final Flaw Size		Initial Flaw Size		Final Flaw Size	
	Depth (a) (in)	a/t	Depth (a) (in)	a/t	Depth (a) (in)	a/t	Depth (a) (in)	a/t
5	0.210	0.1000	0.2103	0.1001	0.210	0.1000	0.2111	0.1005
10	0.500	0.1000	0.5139	0.1028	0.500	0.1000	0.5112	0.1022
11	0.370	0.1000	0.3789	0.1024	0.370	0.1000	0.3768	0.1018
12	0.250	0.1000	0.2542	0.1017	0.250	0.1000	0.2531	0.1012
13	0.220	0.1000	0.2250	0.1023	0.220	0.1000	0.2228	0.1013

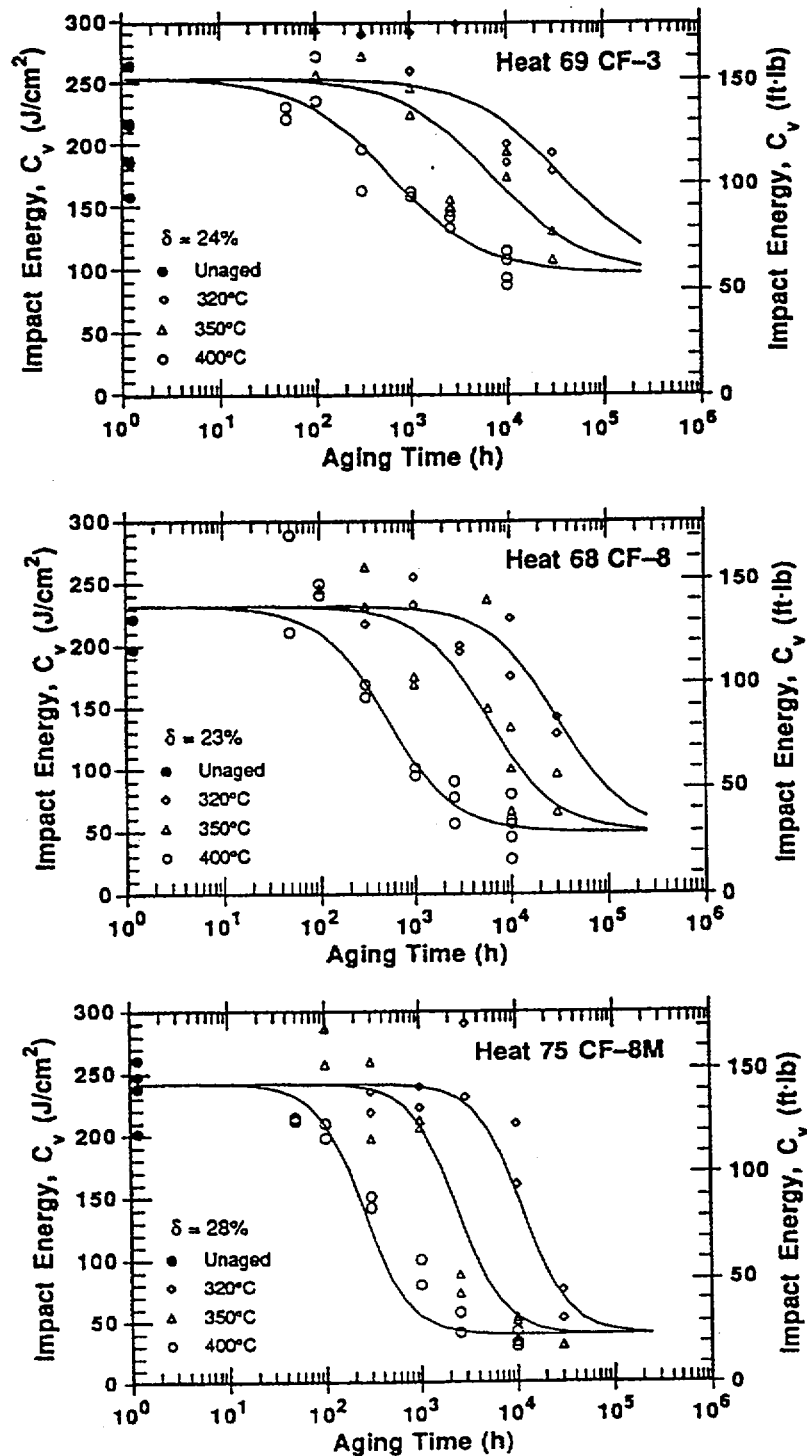


Figure 4-1. Effect of Thermal Aging on Room Temperature Impact Energy of CF3, CF8 and CF8M Cast Stainless Steel [15]

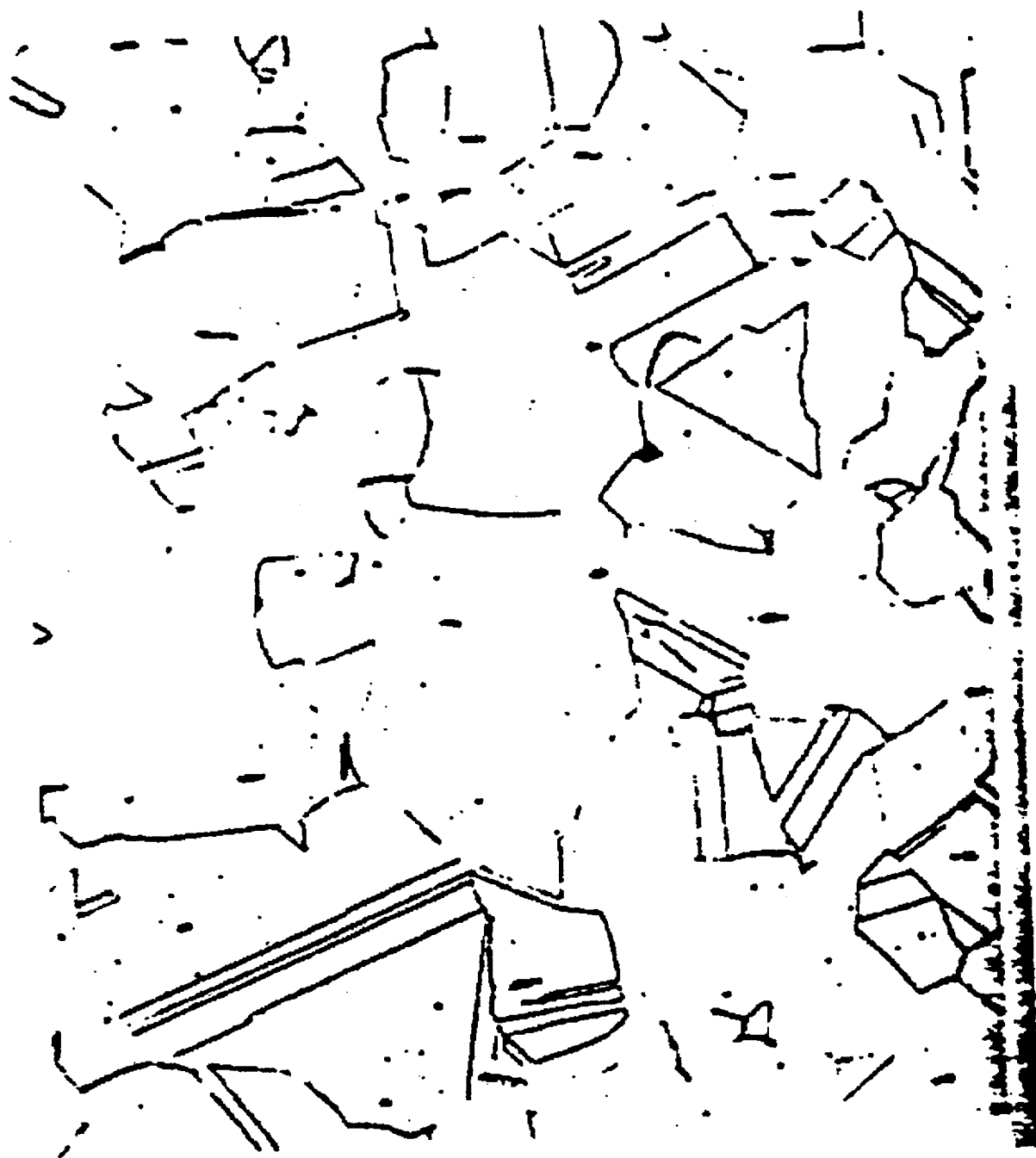


Figure 4-2. Microstructure of Solution Heat Treated Wrought Type 316 Stainless Steel





Figure 4-3. Microstructure of Solution Heat Treated Grade CF8 Stainless Steel Casting  
(Showing Ferrite Phase in Austenitic Matrix)

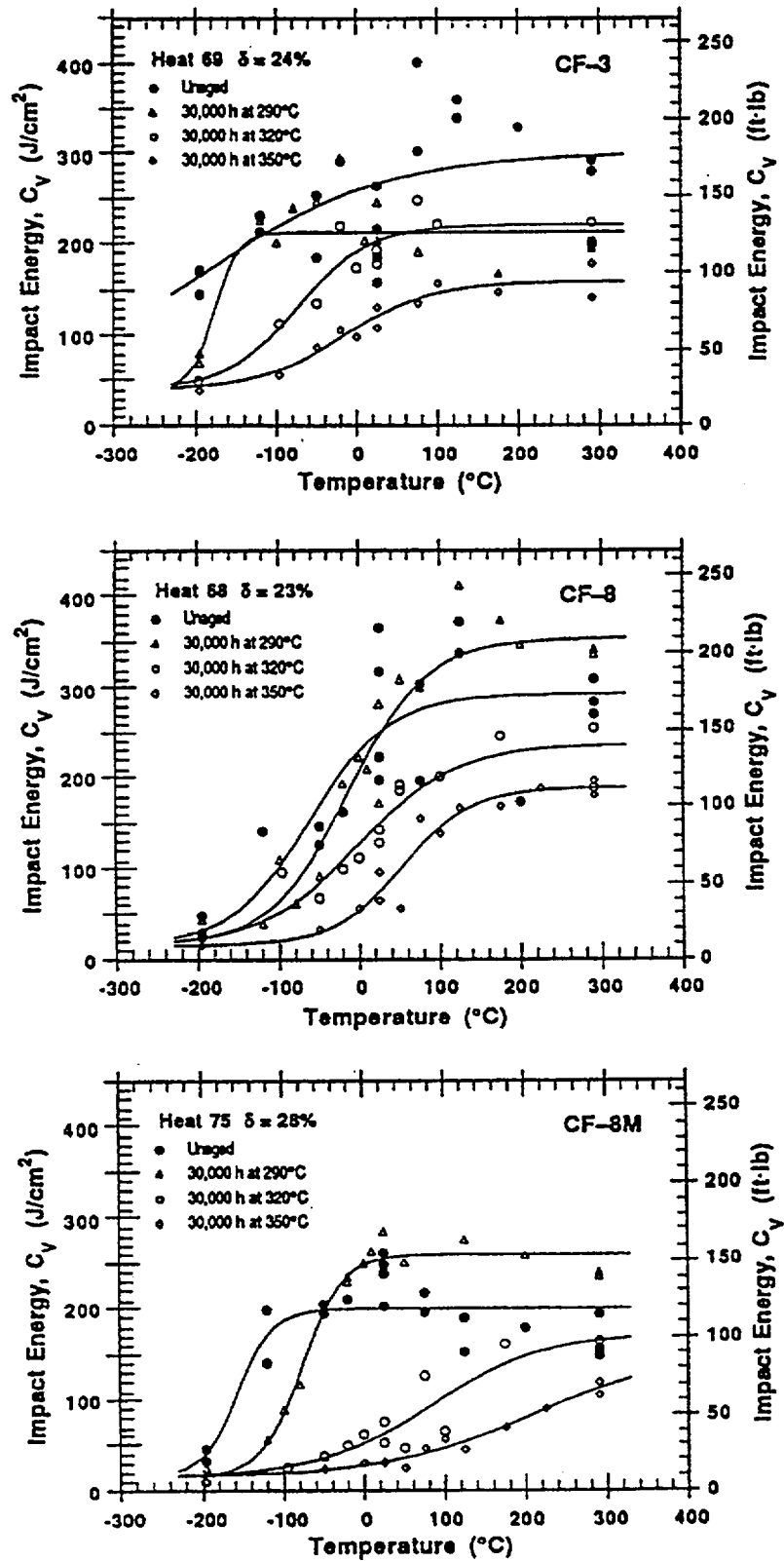


Figure 4-4. Effect of Temperature on Charpy Transition Curves of CF3, CF8 and CF8M Steels Aged for 30,000 hours [15]

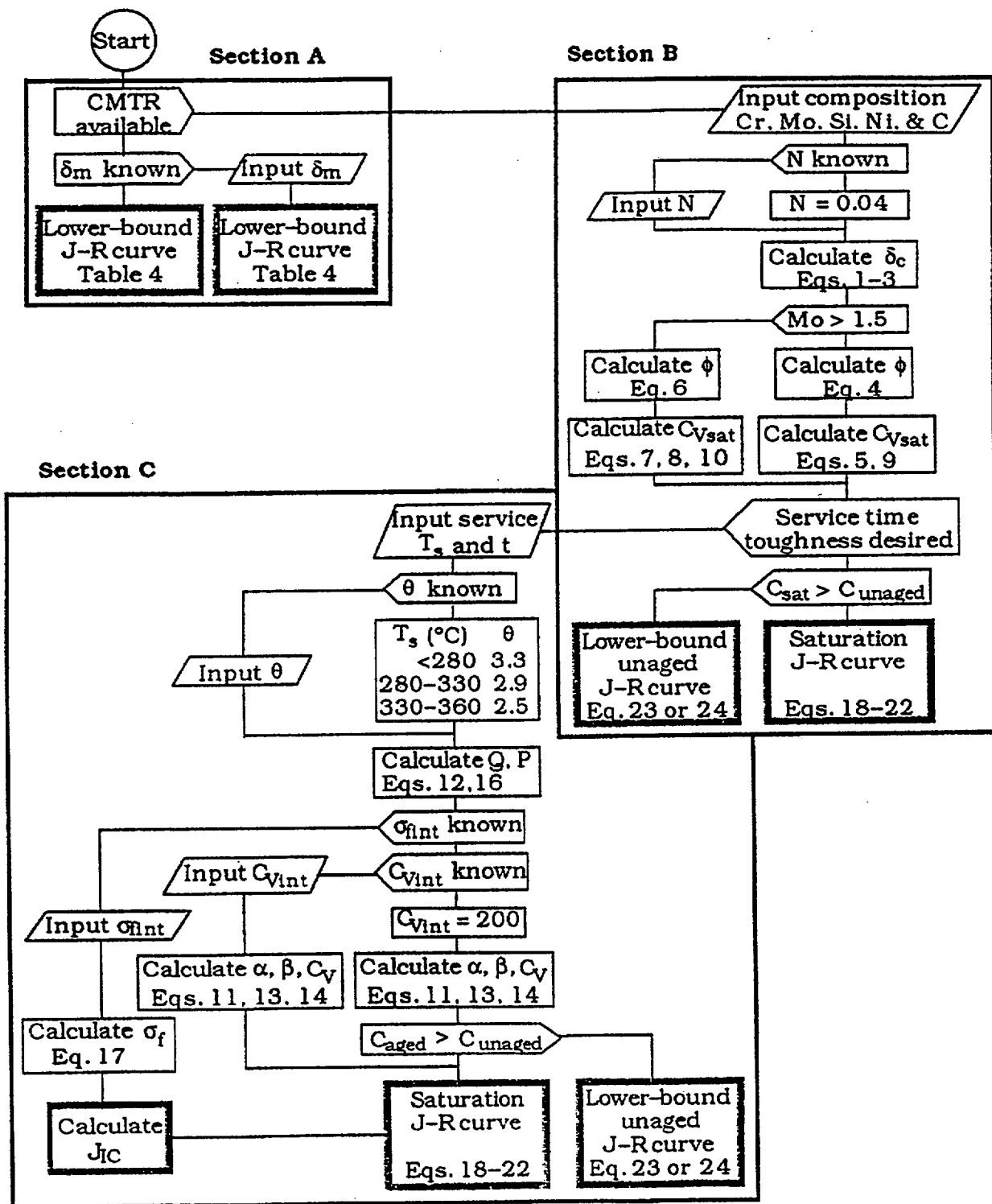


Figure 4-5. Flow Diagram for Estimating Mechanical Properties of Aged Cast Stainless Steels in LWR Systems [21]

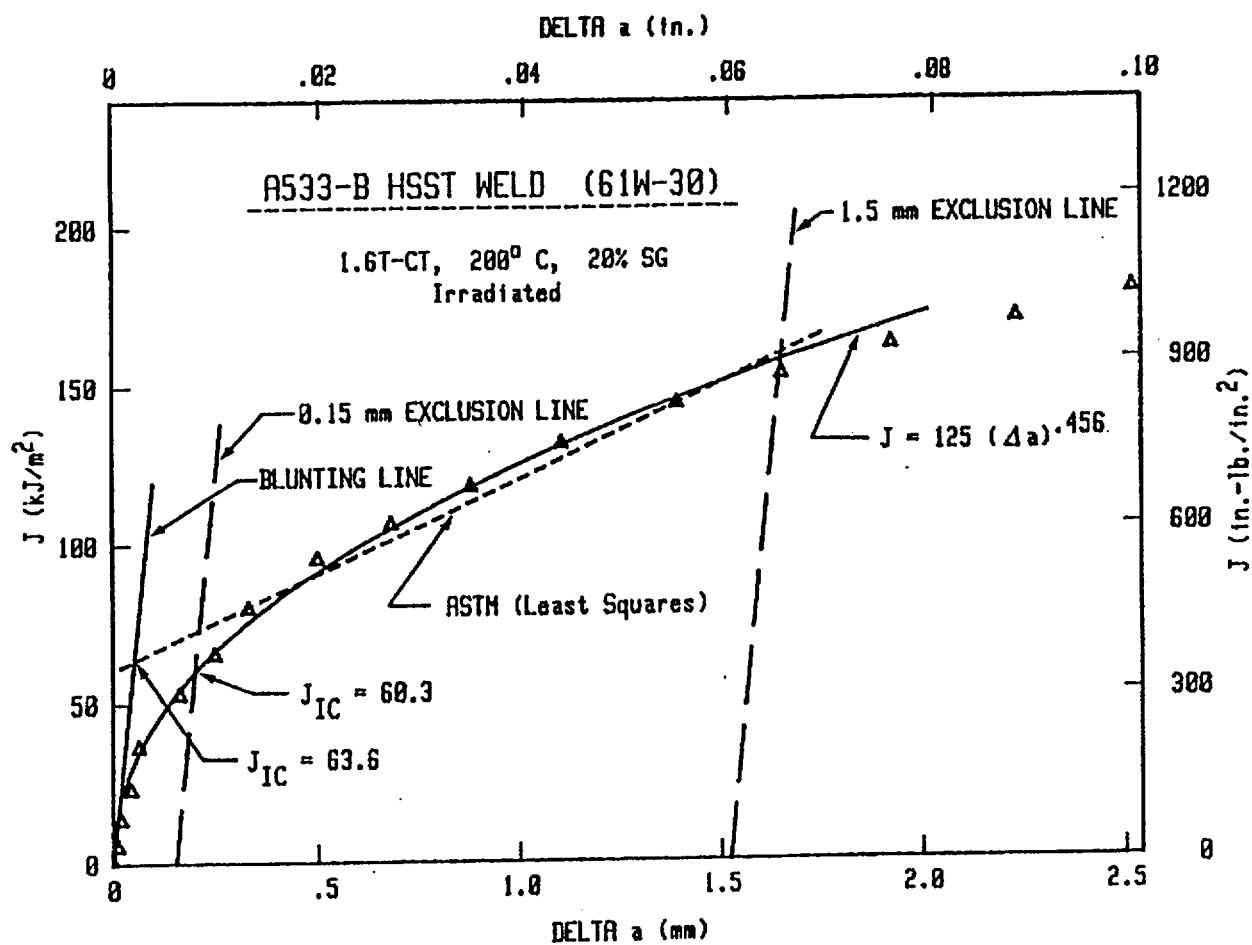


Figure 4-6. Example of a Typical J-R Curve and Determination of  $J_{IC}$  Using the ASTM E 813-81 Methodology [14]

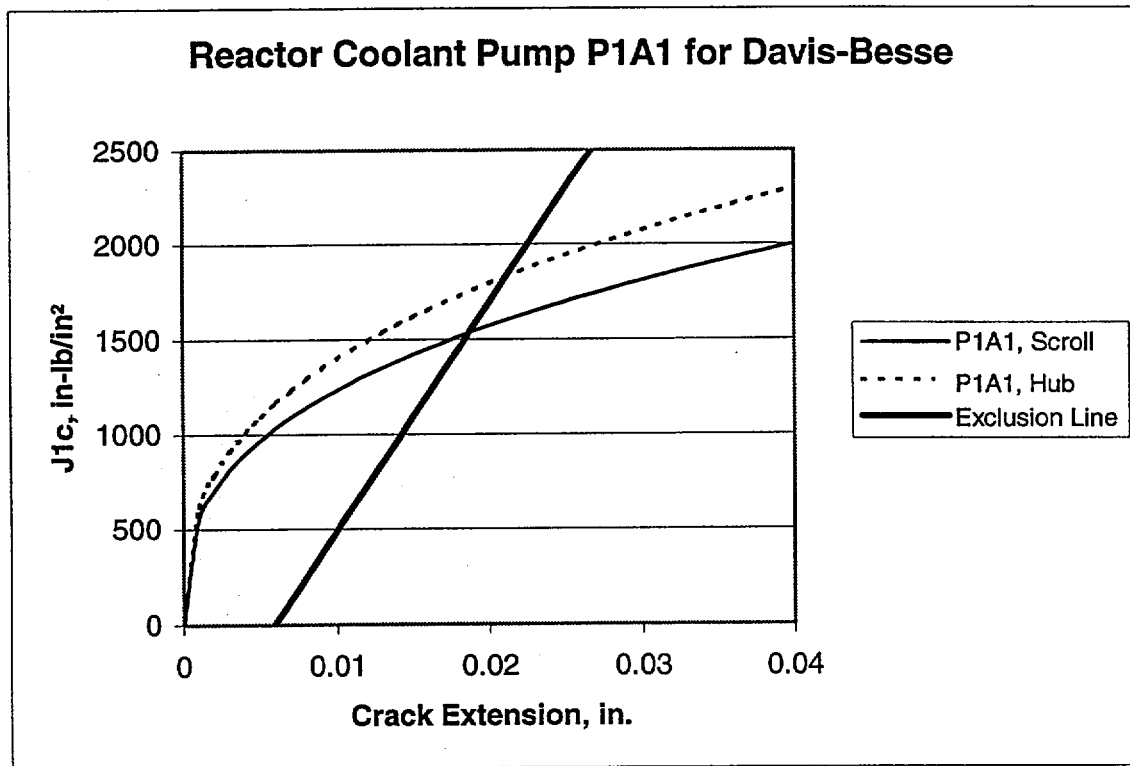


Figure 4-7. Determination of  $J_{1c}$  for Davis-Besse Reactor Coolant Pump 1A1 Casing



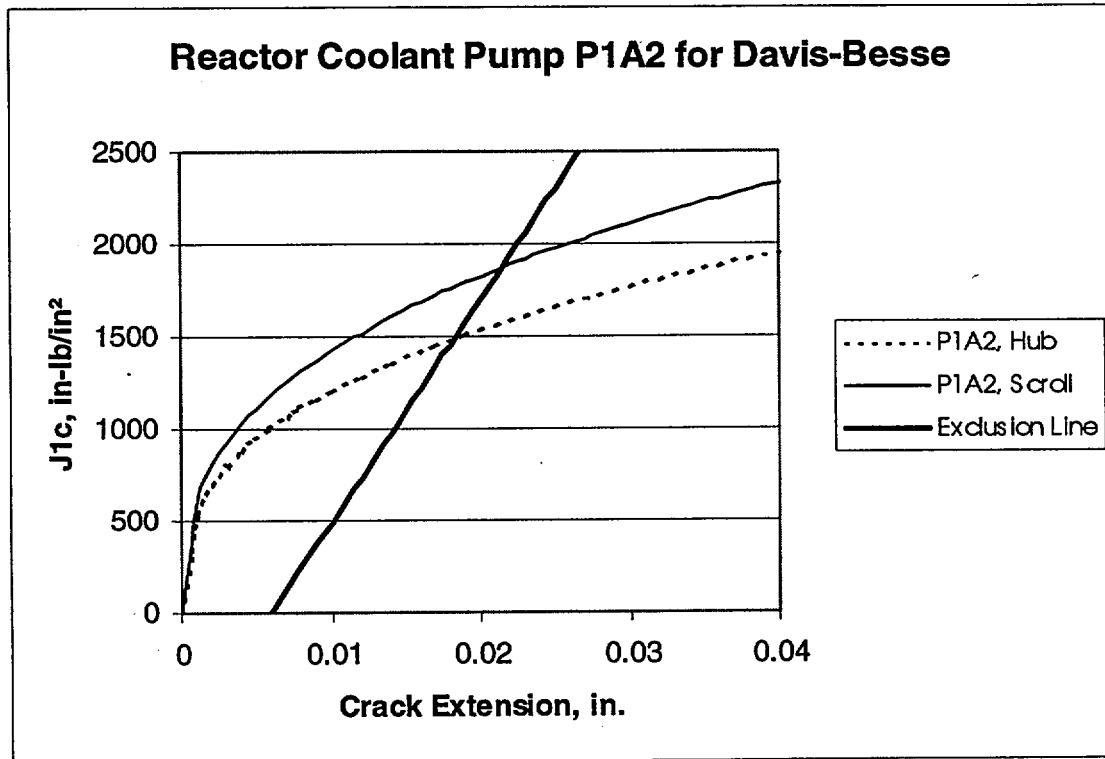


Figure 4-8. Determination of  $J_{1c}$  for Davis-Besse Reactor Coolant Pump 1A2 Casing

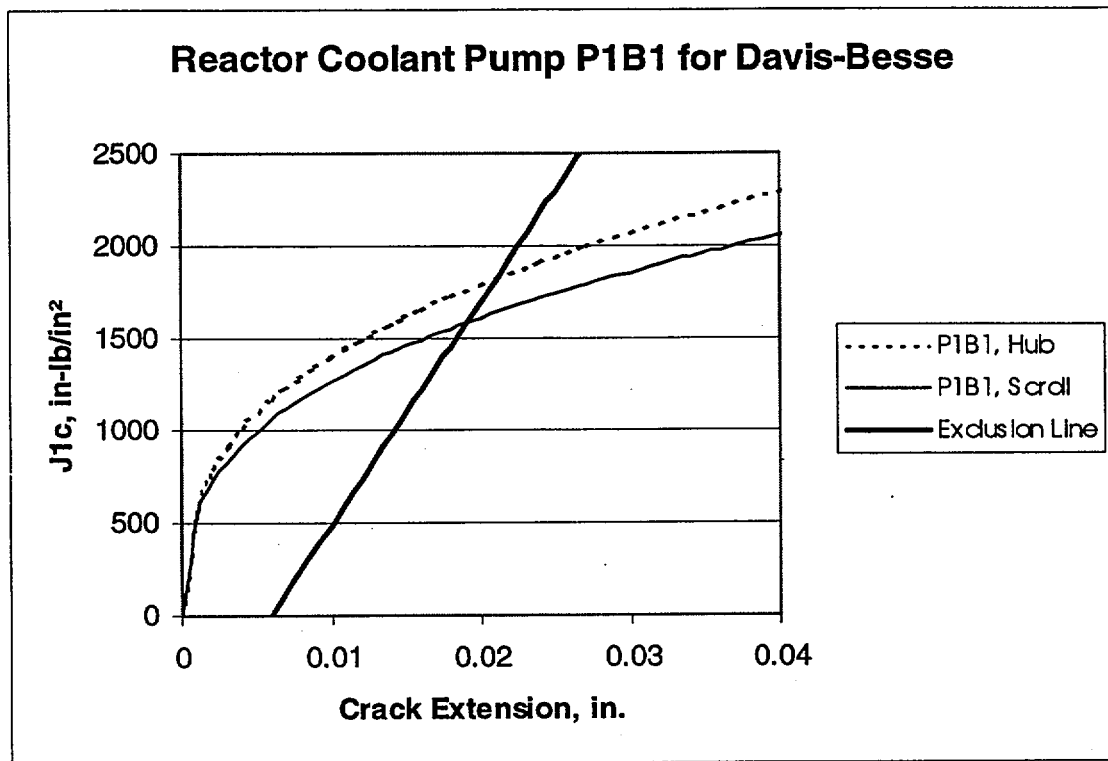


Figure 4-9. Determination of  $J_{1c}$  for Davis-Besse Reactor Coolant Pump 1B1 Casing

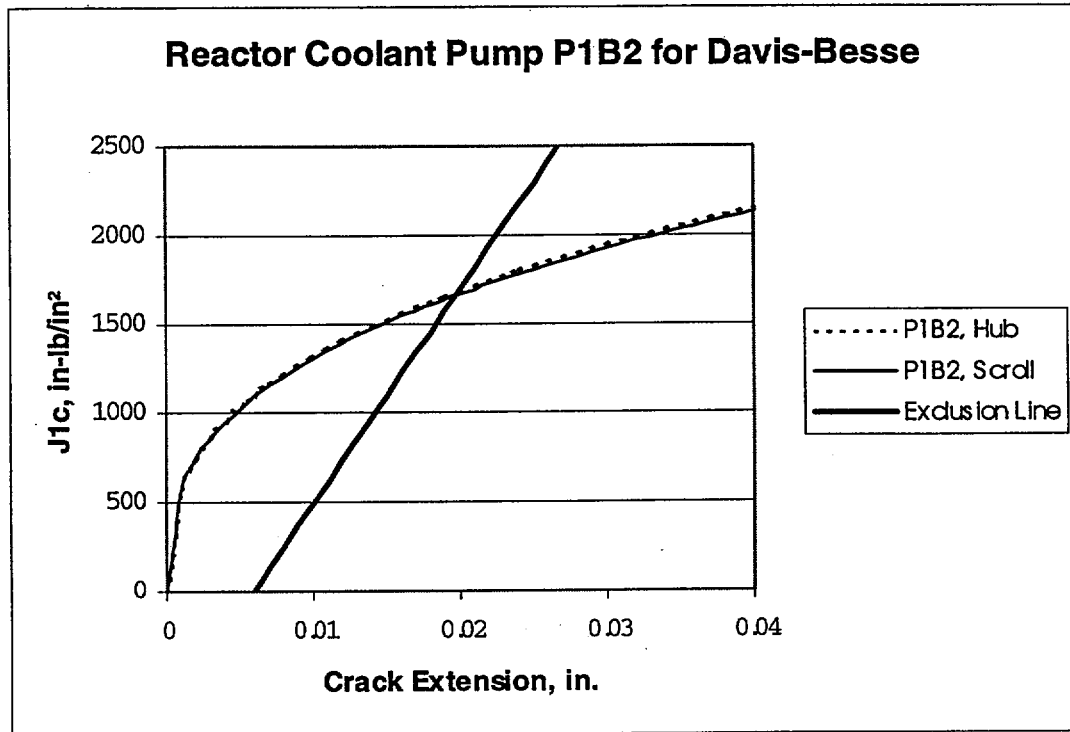


Figure 4-10. Determination of  $J_{1c}$  for Davis-Besse Reactor Coolant Pump 1B2 Casing



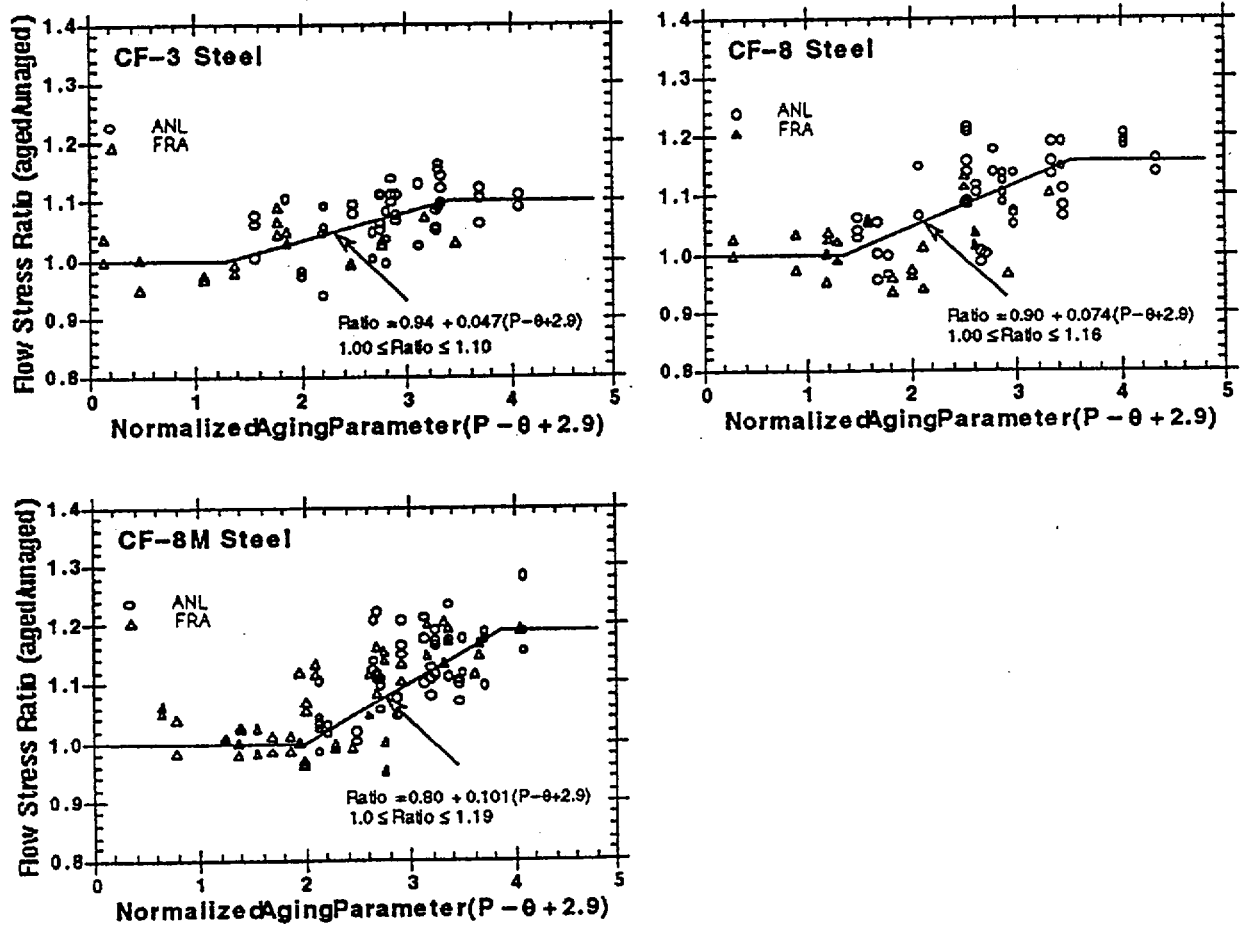


Figure 4-11. Flow Stress Ratio of Aged Cast Stainless Steels at Room Temperature as a Function of Normalized Aging Parameter [21]

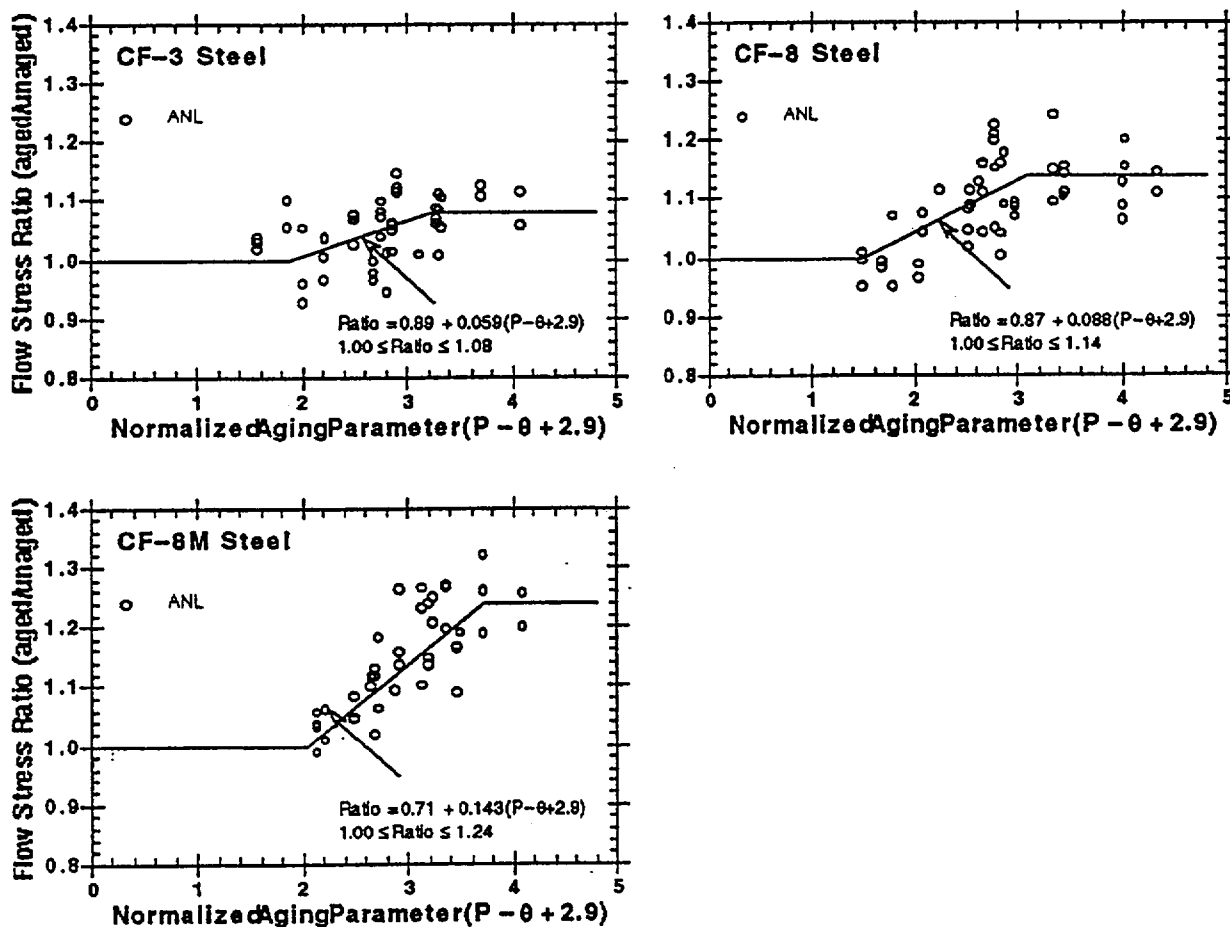


Figure 4-12. Flow Stress Ratio of Aged Cast Stainless Steels at 290 C as a Function of Normalized Aging Parameter [21]

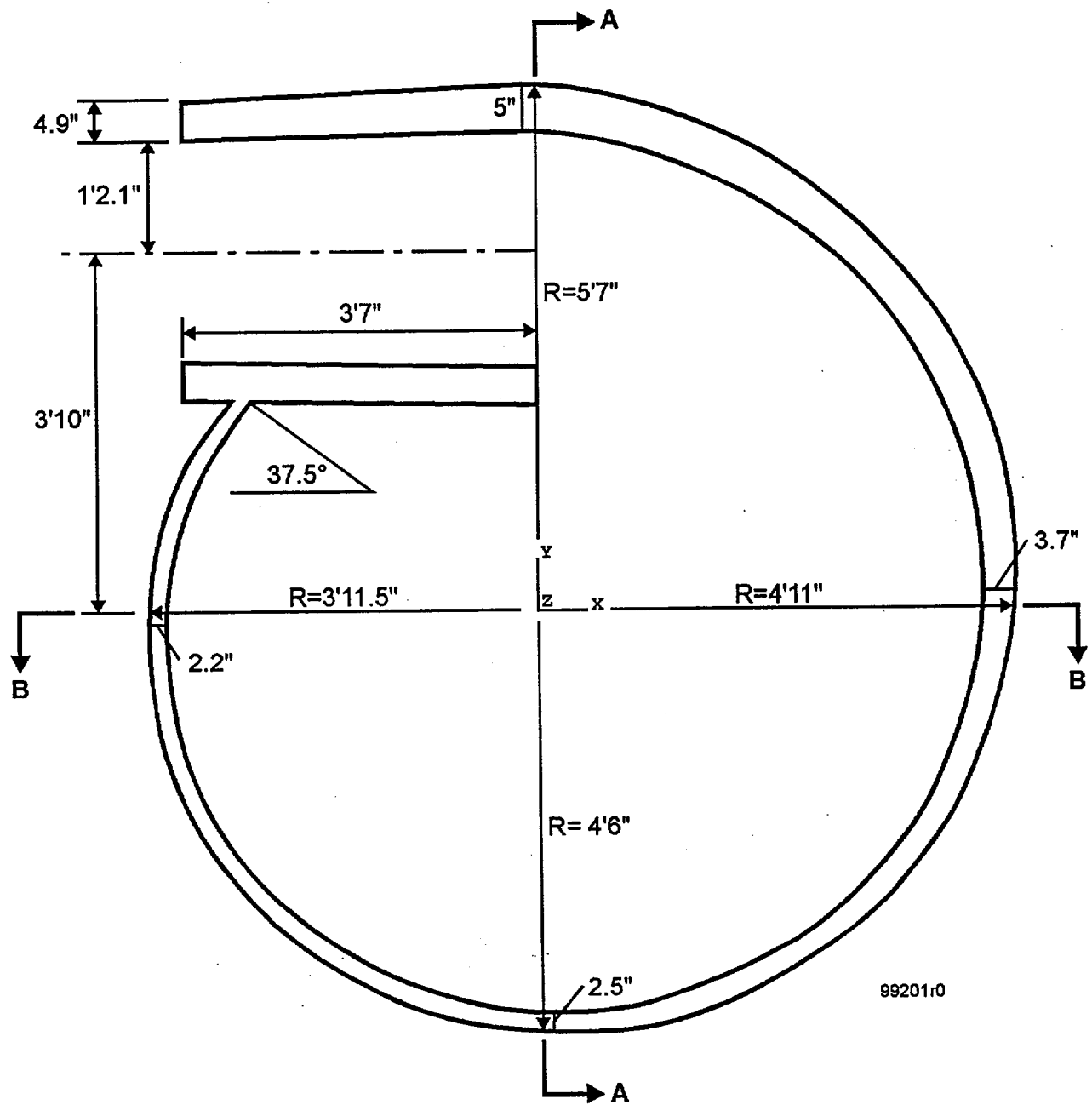


Figure 4-13. Dimensions Used for Finite Element Model for Davis-Besse Pump Casings (Part 1)

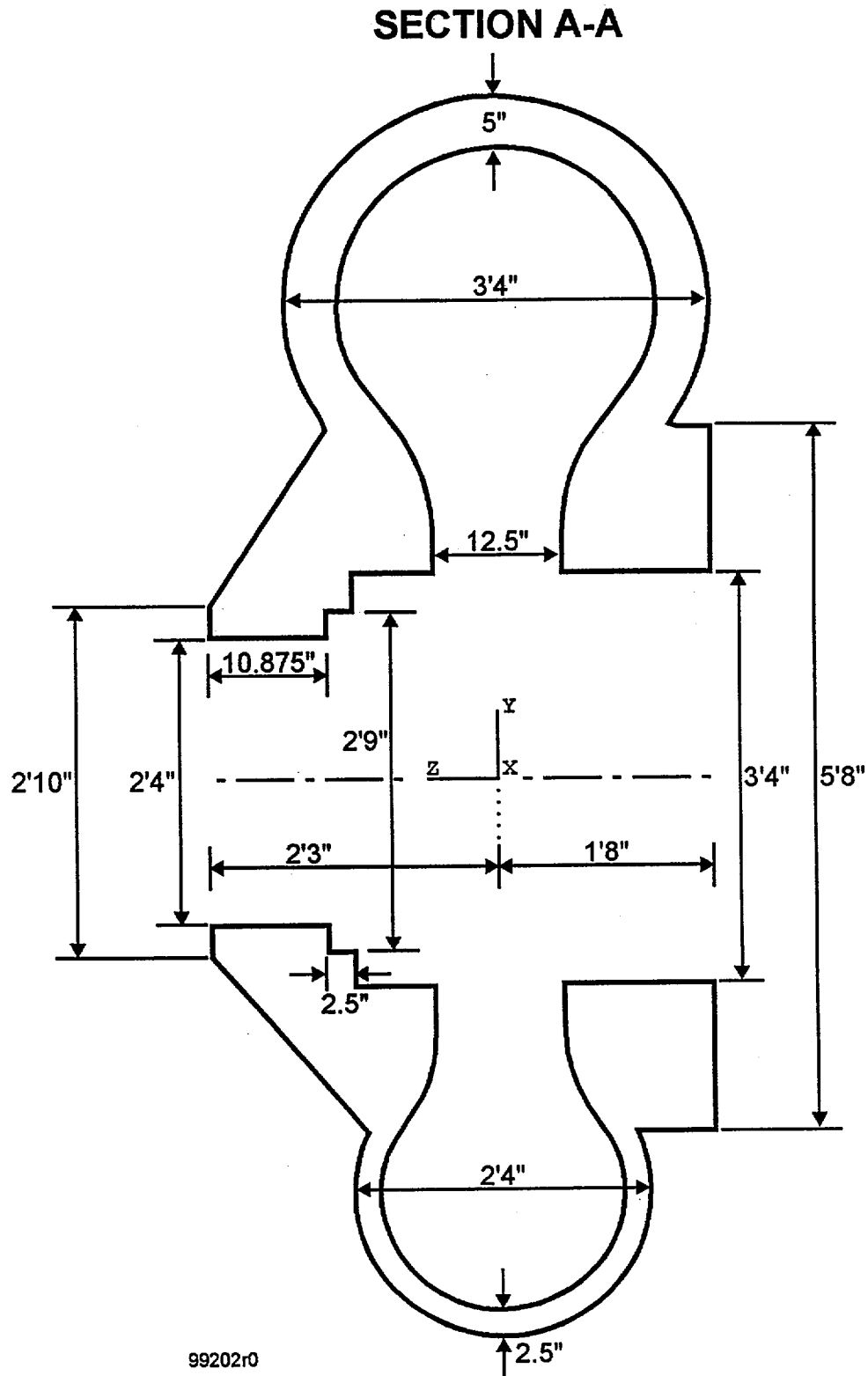
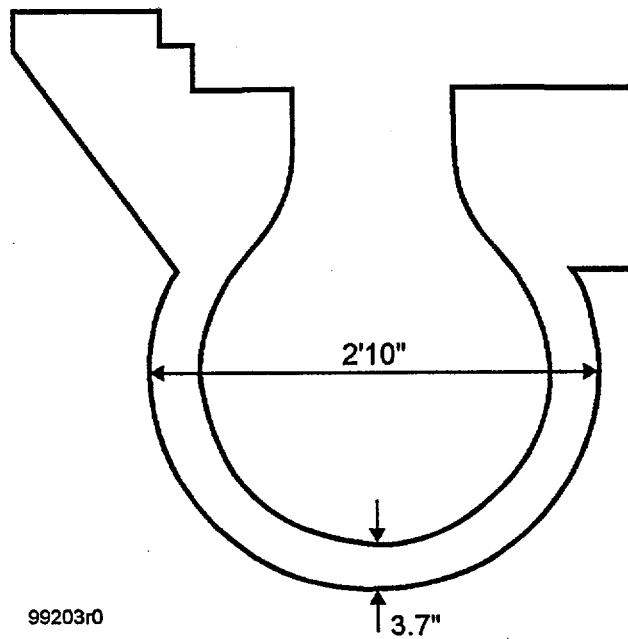
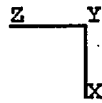
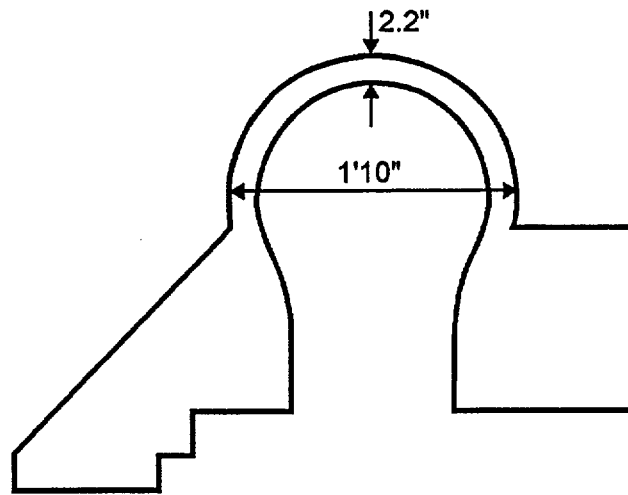


Figure 4-14. Dimensions Used for Finite Element Model for Davis-Besse Pump Casings (Part 2)

## SECTION B-B



99203r0

Figure 4-15. Dimensions Used for Finite Element Model for Davis-Besse Pump Casings (Part 3)

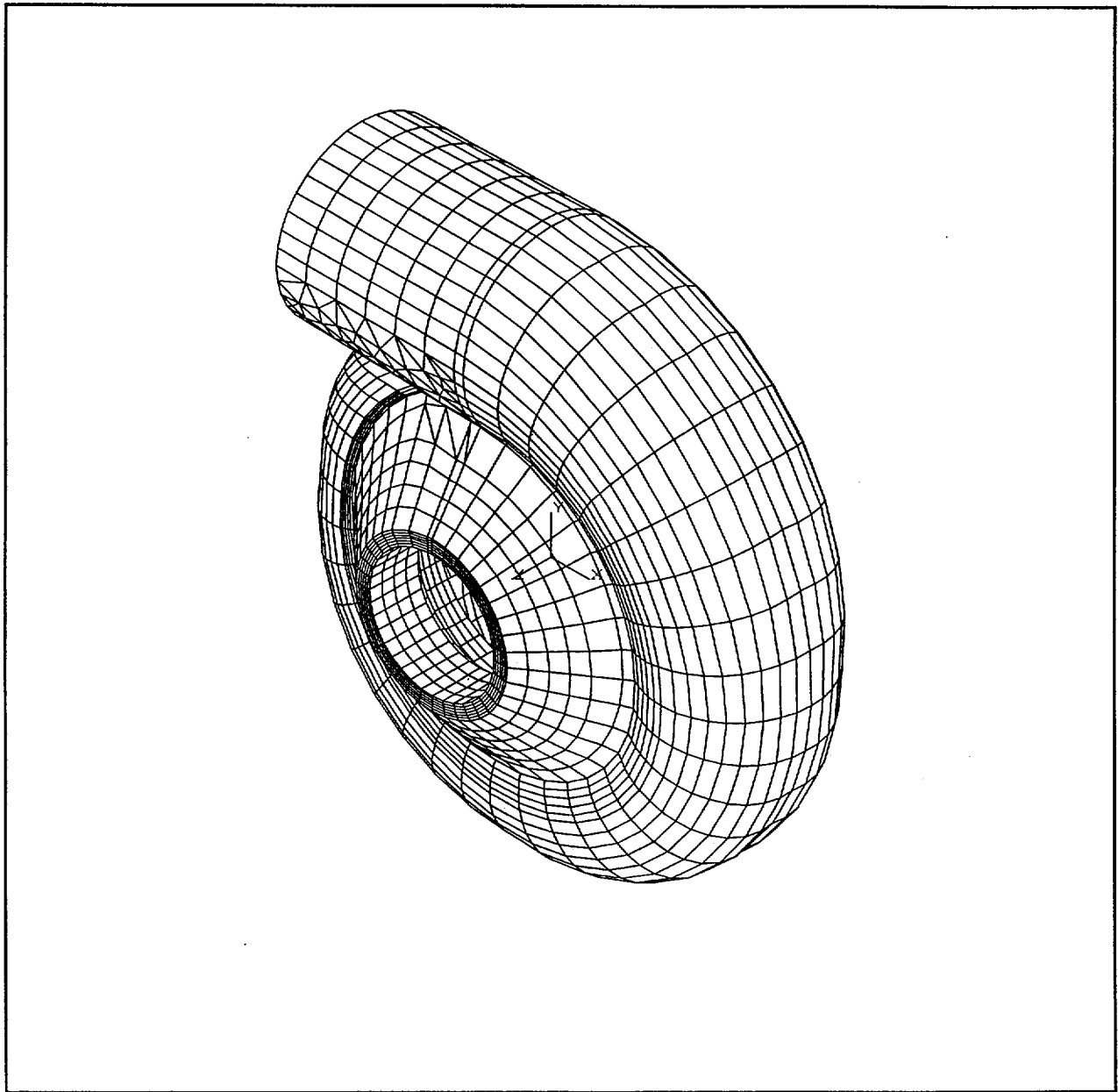


Figure 4-16. Overall Finite Element Model for Davis-Besse Pump Casings (Part 1)

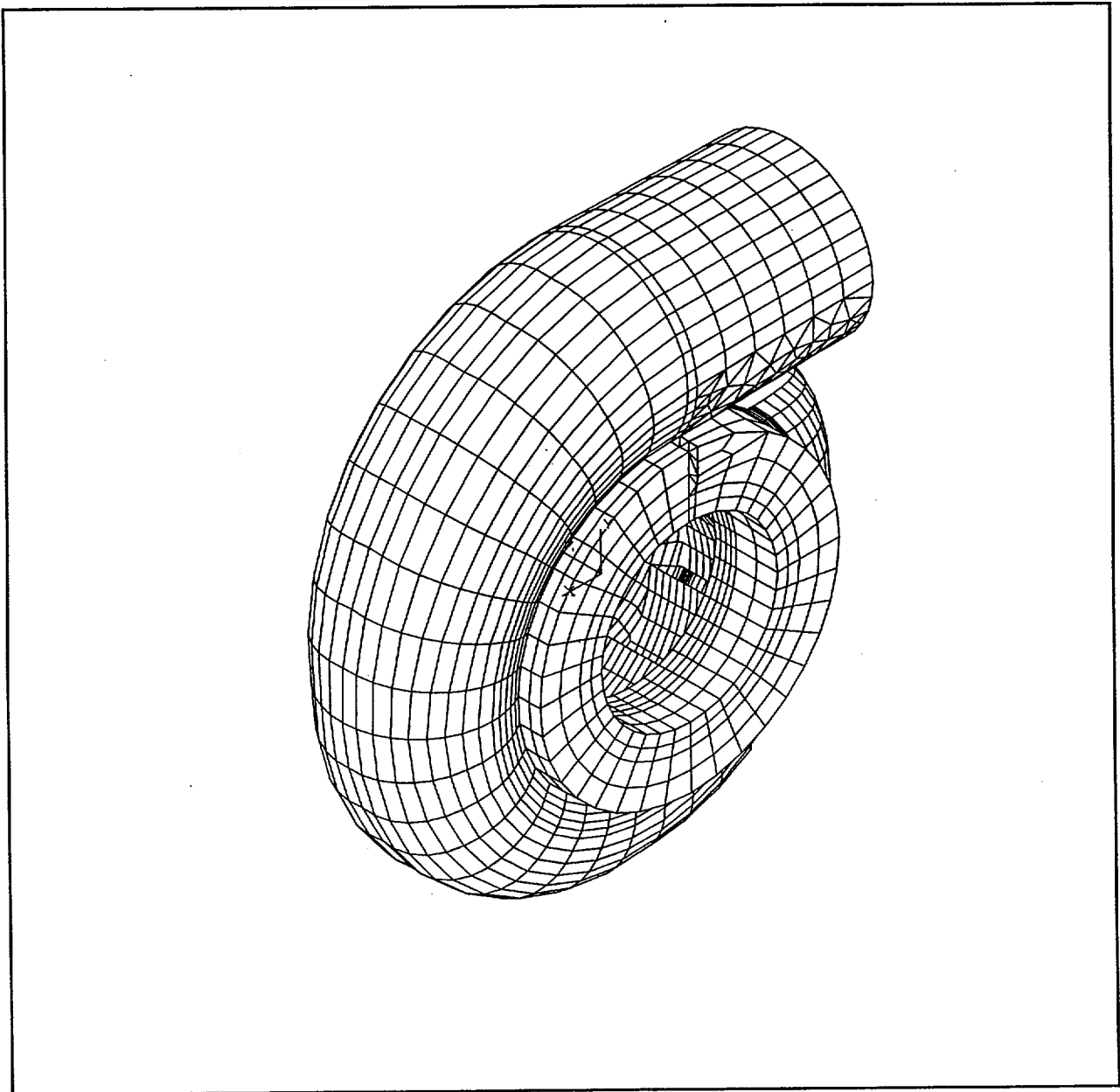


Figure 4-17. Overall Finite Element Model for Davis-Besse Pump Casings (Part 2)

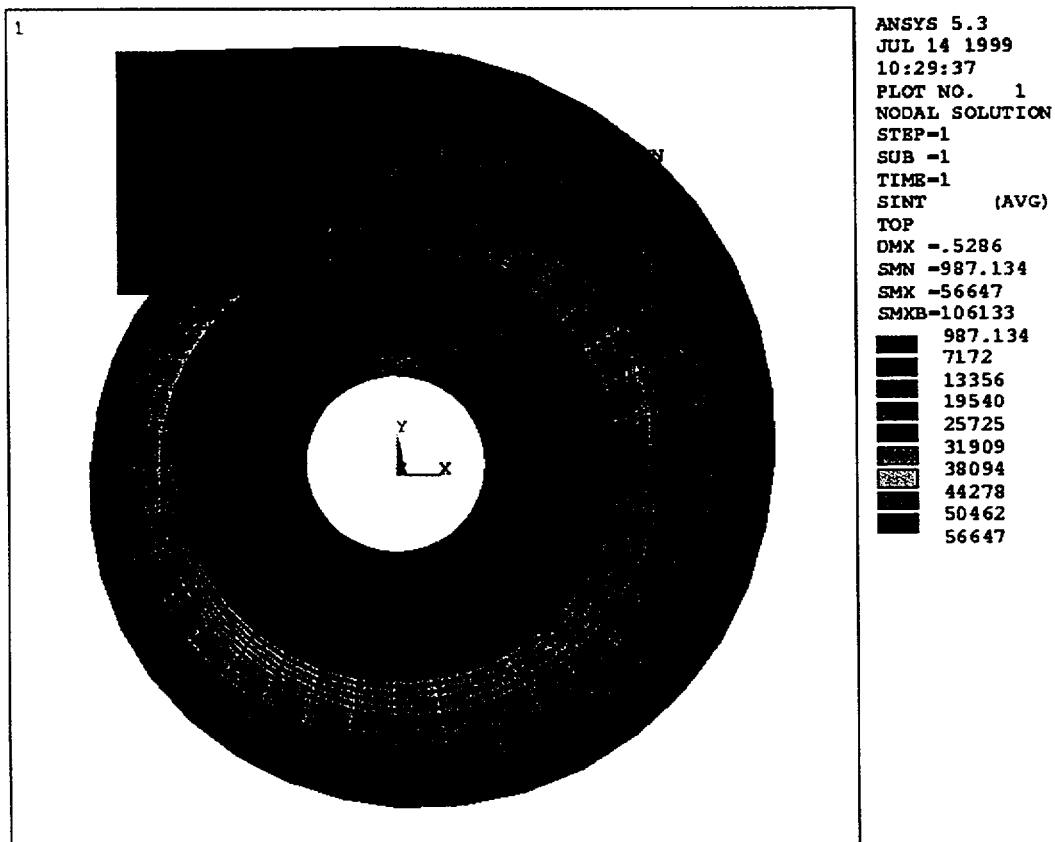


Figure 4-18. Stress Intensity Distribution Due to Internal Pressure of 2250 psig



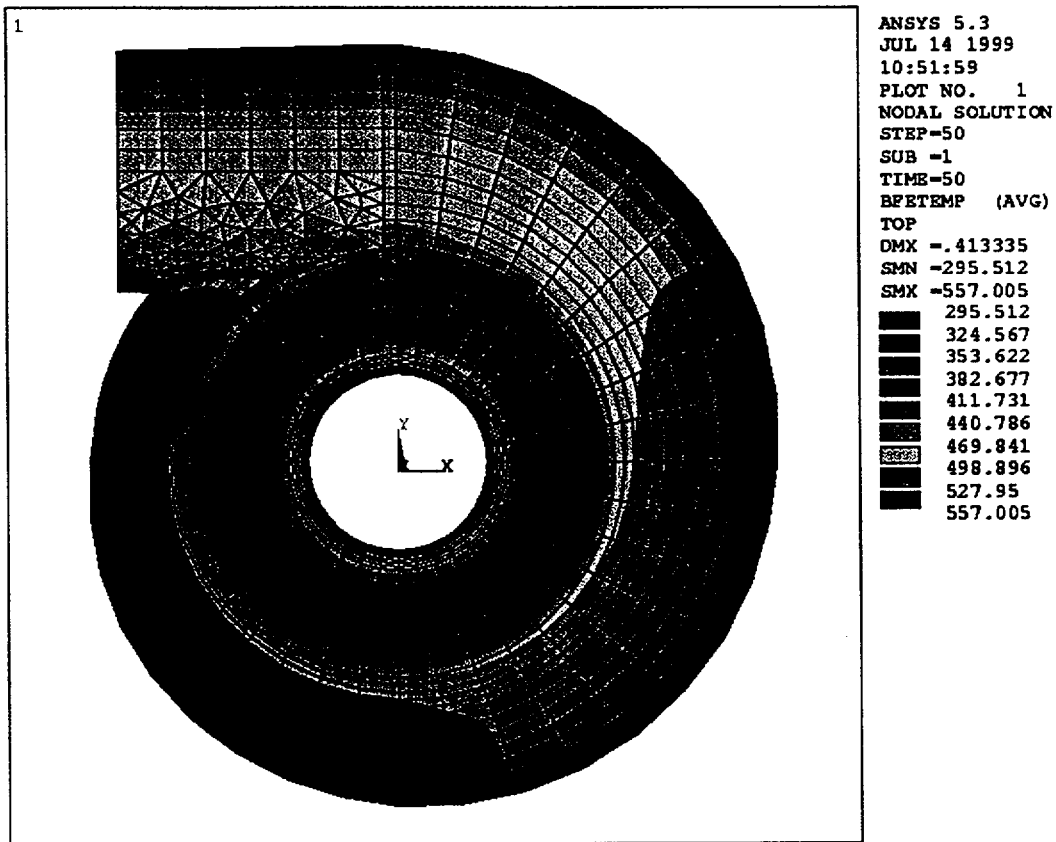


Figure 4-19. Critical Temperature Distribution During Heatup

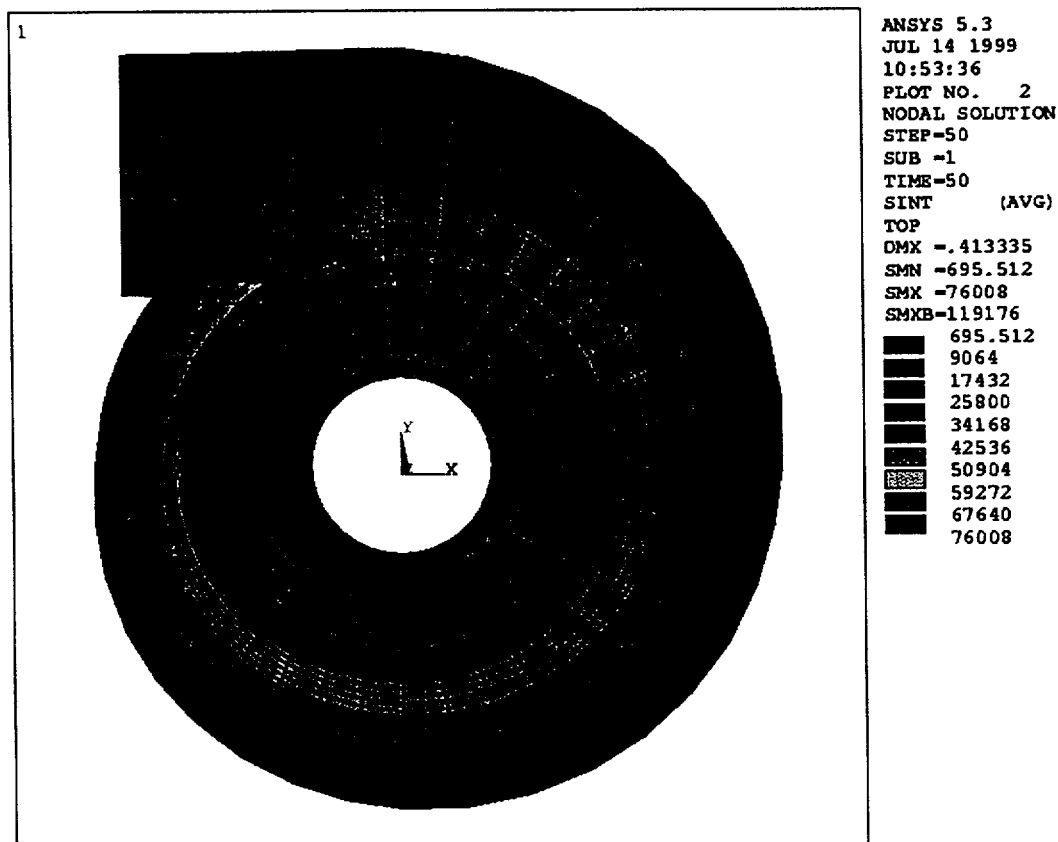


Figure 4-20. Critical Stress Distribution During Heatup

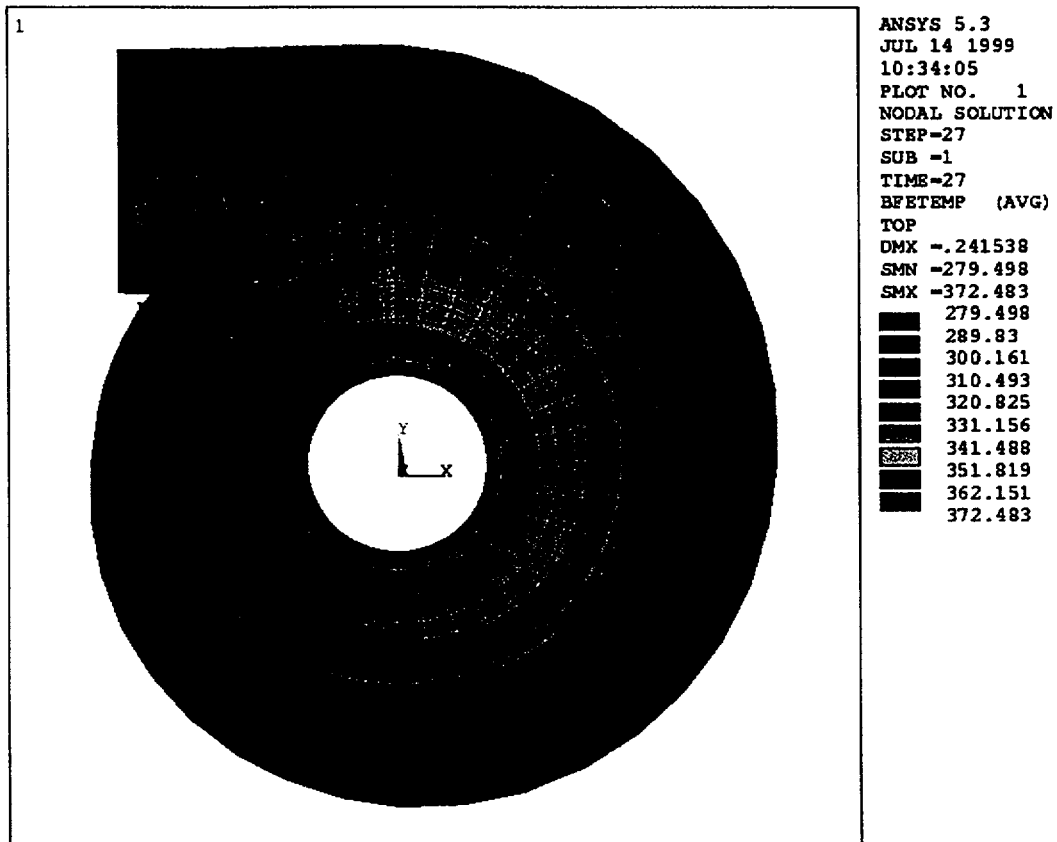


Figure 4-21. Critical Temperature Distribution During Cooldown

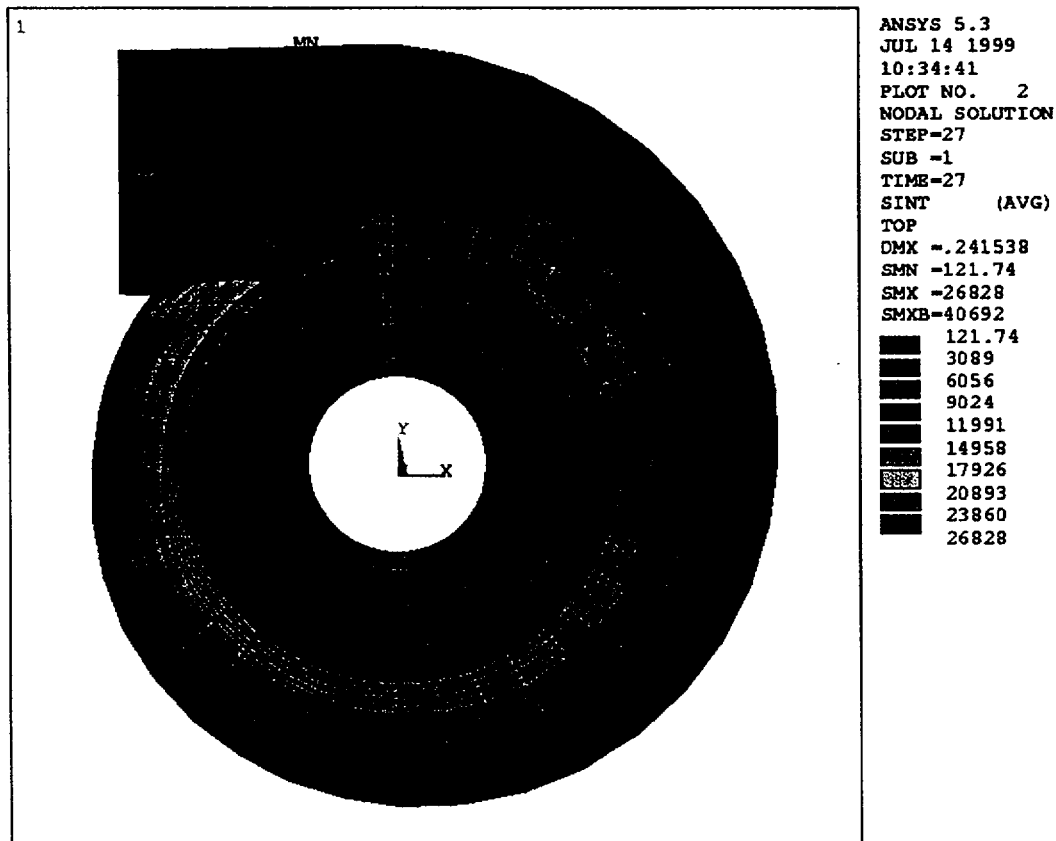


Figure 4-22. Critical Stress Distribution During Cooldown

### Crack Growth (Path 13)

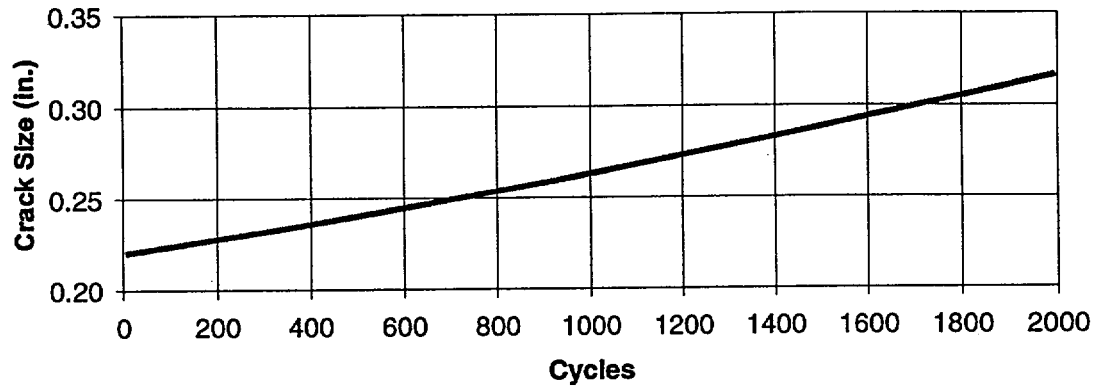


Figure 4-23. Results of Fatigue Crack Growth Analysis for Davis-Besse Pump Casing

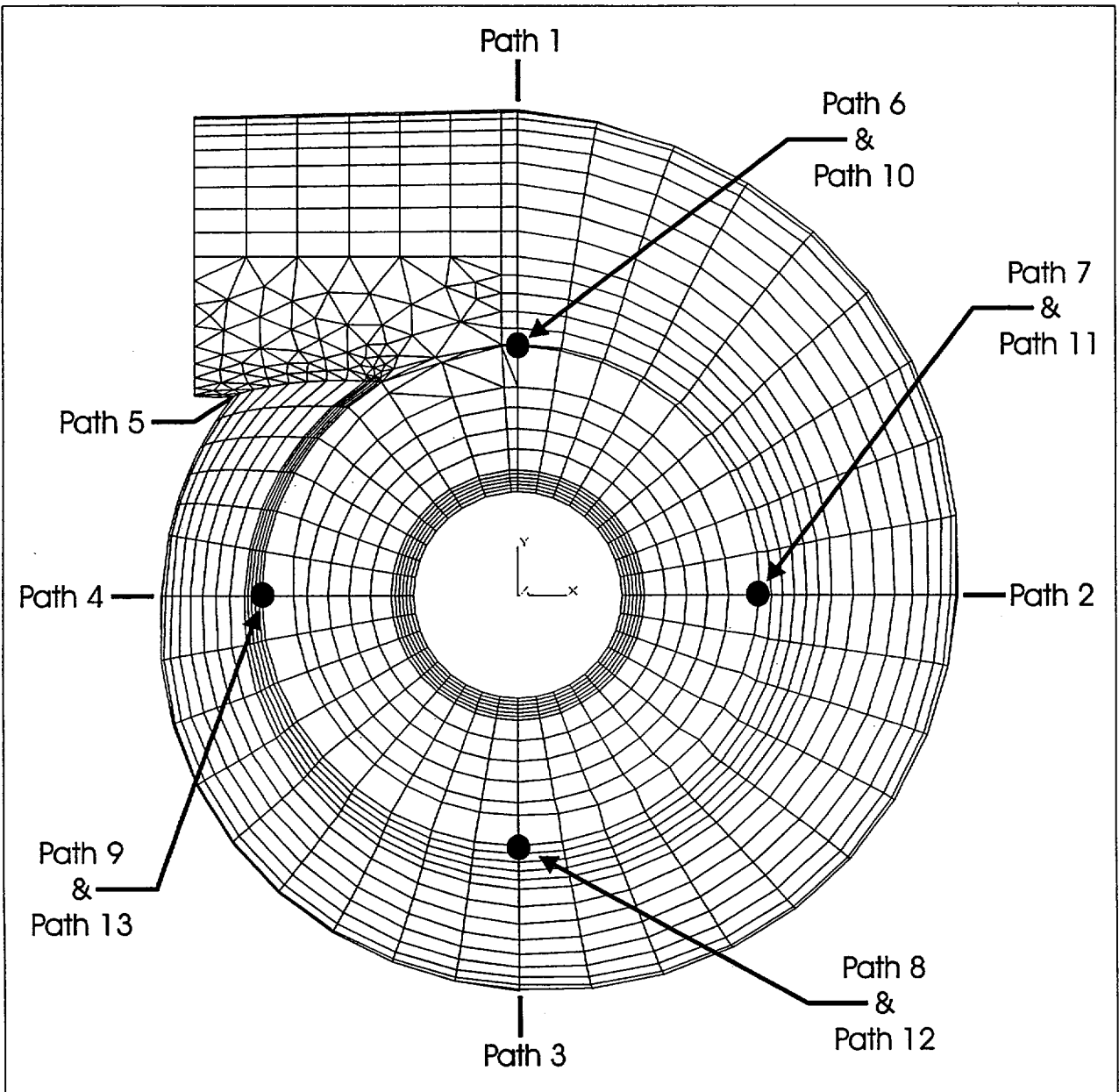


Figure 4-24. Critical Path Locations (1 of 2)

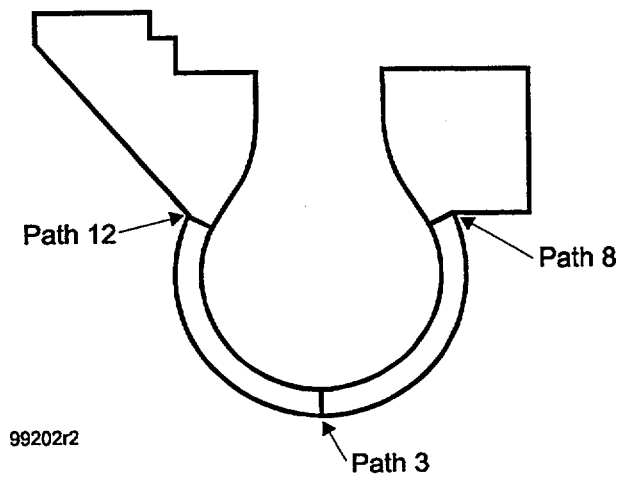
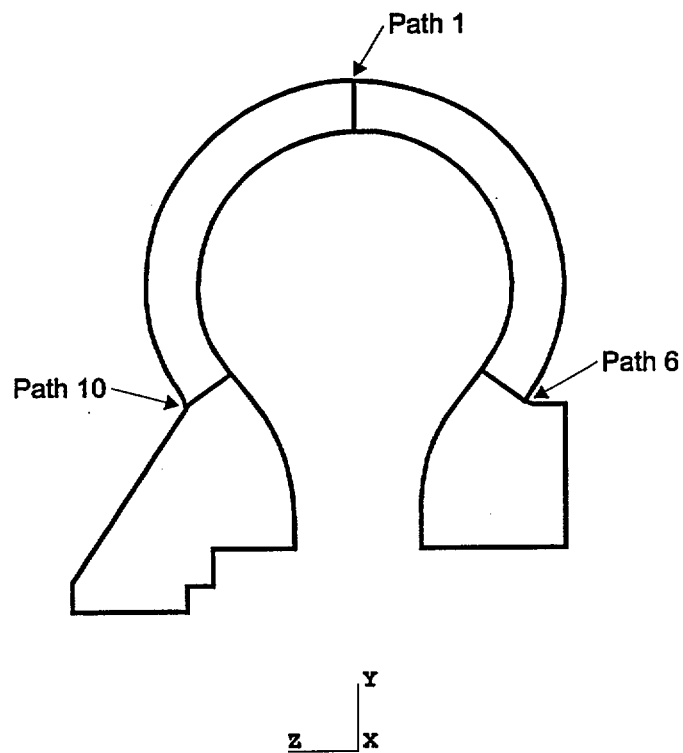


Figure 4-25. Critical Path Locations (2 of 2)

## 5.0 SUMMARY AND CONCLUSIONS

The evaluations contained in this report have demonstrated that the Davis-Besse reactor coolant pump casings meet the safety and serviceability requirements of ASME Code Case N-481.

Highlights of these evaluations are provided as follows:

- The fracture toughness of the base material stainless steel, ASTM A351, Grade CF8M casting, and the weld metal were addressed, including thermal embrittlement considerations. A lower bound fracture toughness of  $139.0 \text{ ksi} \sqrt{\text{in}}$  was used in the analysis.
- Thirteen most highly-stressed locations were chosen as the critical locations for evaluation based on finite element analyses performed for operating pressure and heatup/cooldown transients.
- Flaws were postulated both in the axial and hoop directions at the critical locations and the corresponding normal stresses were used in the fracture mechanics evaluation.
- Consistent with similar evaluations for pressure vessels with postulated large flaws, per Appendix G of ASME Code, Section III, safety factors of 2 for primary and 1 for secondary loads were used for Service Levels A and B conditions. At the critical locations, the applied stress intensity factors were below the allowable values. The stress intensity factors at these locations ranged from  $-1.9$  to  $77.8 \text{ ksi} \sqrt{\text{in}}$  compared to the allowable of  $139.0 \text{ ksi} \sqrt{\text{in}}$ .

Fatigue crack growth analysis was performed assuming an initial flaw size corresponding to the acceptance standards of ASME Code, Section XI, and considering all the significant plant transients. The analysis indicated that fatigue crack growth is very small (initial 10% through-wall flaw grows to 10.3% during 40 year plant life involving 240 heatup/cooldowns). After 2000 cycles, the initial 10% through-wall flaw has grown to only 15%, indicating that the quarter thickness flaw bounds any flaw that may be identified during service.





## 6.0 REFERENCES

1. ASME Boiler and Pressure Vessel Code, Code Case N-481, "Alternate Examination Requirements for Cast Austenitic Pump Casings, Section XI, Division 1", March 5, 1990.
2. ASME Boiler and Pressure Vessel Code, Section III, 1968 Edition, 1968 Winter Addenda.
3. Babcock and Wilcox Specification No. 1036/0569, dated May 23, 1969, Revision SC-184, Appendix "C" and "D" dated December 15, 1972.
4. Byron Jackson Report No. TCI-7020-STR, Vol. 1, Revision 1, "Case Stress Analysis, 33x33x38 DFSS Primary Coolant Pump, Toledo Edison Company," dated September 9, 1976.
5.
  - a. Babcock and Wilcox, Baseline Examination for 1A1, 1A2, 1B1, 1B2 Pump Casing Welds, Contract No. 192-051-000, January through March 1975, SI File TECO-07Q-203.
  - b. Babcock and Wilcox, Repair of Reactor Coolant Pump Casing P1A1, P1A2, P1B1, P1B2, Contract No. 620-0014, July through September 1975, SI File No. TECO-07Q-204.
6. B&W Nuclear Service Company, "1990 Volumetric Examination Results of Reactor Coolant Pump 1-2-1 for Toledo Edison Company Davis-Besse Unit 1," Revision 0, Outage No. 6, Reference No. 580-7624, Task 1091, June 1990, SI File No. TECO-07Q-207.
7. EPRI Report TR-100034, "Cast Austenitic Stainless Steel Sourcebook", prepared by EPRI and Structural Integrity Associates, October 1991.
8. "Safety Evaluation by the Office of the Nuclear Reactor Regulation Related to the Inservice Inspection (ISI) Program, Arkansas Power and Light Company, Arkansas Nuclear One, Unit 1, Docket No. 50-313", dated April 25, 1989. Attached to letter from Mr. J. A. Calvo (NRC) to Mr. T. G. Campbell (AP&L), "Reactor Coolant Pump Casing Weld Flaw Indications - Request for Relief from ASME Section XI Inspection Requirements, Arkansas Nuclear One, Unit 1 (TAC No. 64146)", dated April 25, 1989.
9. O. K. Chopra and H. M. Chung, Long-Term Embrittlement of Cast Duplex Stainless Steels in LWR Systems: Semiannual Report, April-September 1987, NUREG/CR-4744 Vol. 2, No. 2, ANL-89/6 (August 1989).
10. O. K. Chopra and H. M. Chung, Long-Term Embrittlement of Cast Duplex Stainless Steels in LWR Systems: Semiannual Report, October 1987-March 1988, NUREG/CR-4744 Vol. 3, No. 1, ANL-89/22 (February 1990).



11. O. K. Chopra and H. M. Chung, Long-Term Embrittlement of Cast Duplex Stainless Steels in LWR Systems: Semiannual Report, April-September 1988, NUREG/CR-4744 Vol. 3, No. 2, ANL-90/5 (August 1990).
12. O. K. Chopra and H. M. Chung, Long-Term Embrittlement of Cast Duplex Stainless Steels in LWR Systems: Semiannual Report October 1988-March 1989, NUREG/CR-4744, Vol. 4, No. 1, ANL-90/44 (May 1991).
13. O. K. Chopra, A. Sather, and L. Y. Bush, Long-Term Embrittlement of Cast Duplex Stainless Steels in LWR Systems: Semiannual Report April-September 1989, NUREG/CR-4744, Vol. 4, No. 2, ANL-90/49 (June 1991).
14. A. L. Hiser, Tensile and J-R Curve Characterization of Thermally Aged Cast Stainless Steels, NUREG/CR-5024, MEA-2229, Materials Engineering Associates, Inc. (September 1988).
15. E. I. Landerman and W. H. Bamford, "Fracture Toughness and Fatigue Characteristics of Centrifugally Cast Type 316 Stainless Steel Pipe after Simulated Thermal Service Conditions", in Ductility and Toughness Considerations in Elevated Temperature Service, MPC 8, ASME, New York, pp. 99-127 (1978).
16. S. Bonnet, J. Bourgoïn, J. Champredonde, D. Guttmann, and M. Guttmann, "Relationship Between Evolution of Mechanical Properties of Various Cast Duplex Stainless Steels and Metallurgical and Aging Parameters: An Outline of Current EDF Programs", Mater. Sci. and Technol., 6, 221-229 (1990).
17. P. H. Pumphrey and K. N. Akhurst, "Aging Kinetics of CF3 Cast Stainless Steel in Temperature Range 300-400 C", Mater. Sci. Technol., 6, 211-219 (1990).
18. G. Slama, P. Petrequin, and T. Mager, "Effect of Aging on Mechanical Properties of Austenitic Stainless Steel Castings and Welds", presented at SMiRT Post-Conference Seminar 6, Assuring Structural Integrity of Steel Reactor Pressure Boundary Components, August 29-30, 1983, Monterey, CA.
19. Y. Meyzaud, P. Ould, P. Balladon, M. Bethmont, and P. Soulat, "Tearing Resistance of Aged Cast Austenitic Stainless Steel", presented at Intl. Conf. on Thermal Reactor Safety (NUCSAFE 88), October 1988, Avignon, France.
20. P. McConnell and J. W. Sheckherd, Fracture Toughness Characterization of Thermally Embrittled Cast Duplex Stainless Steel, Report NP-5439, September 1987, Electric Power Research Institute, Palo Alto, CA.
21. O. K. Chopra, "Estimation of Mechanical Properties of Cast Stainless Steels During Thermal Aging in LWR Systems", NUREG/CP-0119, Vol. 2, pp. 151-178, Proceedings of the U.S. Nuclear Regulatory Commission, 19th Water Reactor Safety Information Meeting held at Bethesda, MD, October 28-30, 1991, published April 1992.



22. L. S. Ambrey, P. F. Wieser, W. J. Pollard, and E. A. Schoefer, "Ferrite Measurement and Control in Cast Duplex Stainless Steel", in *Stainless Steel Castings*, V. G. Behal and A. S. Melilli, editors, ASTM STP 756, pp. 126-164 (1982).
23. Byron Jackson Certification and Fabrication Reports for Pump Serial Nos. 701-N-0592 (Pump A), 701-N-0594 (Pump B), 701-N-0595 (Pump C), and 701-N-0593 (Pump D).
24. ASTM E813 "Standard Test Method for  $J_{Ic}$ , A Measure of Fracture Toughness", American Society for Testing and Materials, Philadelphia, PA.
25. ASME Boiler and Pressure Vessel Code, Section III Appendices, 1989 Edition.
26. EPRI Report NP-4668, "Evaluation of the Toughness of Austenitic Stainless Steel Pipe Weldments", June 1986.
27. EPRI Report NP-4768, "Toughness of Austenitic Stainless Steel Pipe Welds", October 1986.
28. EPRI Report NP-4690-SR, "Evaluation of Flaws in Austenitic Steel Piping", July 1986.
29. ANSYS Linear Plus/Thermal, Revision 5.5.1, ANSYS Inc., October 1998.
30. Byron Jackson Pump Division Drawing No. 2B-12865, "As-Built Dimensions," SI File No. TECO-07Q-201.
31. Byron Jackson Pump Division Drawing No. 2E-1424, Rev. E, "Outline – 33x33x38 DFSS Primary Coolant Pump," SI File TECO-07Q-201.
32. ASME Boiler and Pressure Vessel Code, Section XI, 1989 Edition.
33. **pc-CRACK** Computer Software, Version 3.1, Structural Integrity Associates.
34. Section XI Task Group for Piping Flaw Evaluation, ASME Code, "Evaluation of Flaws in Austenitic Steel Piping", *Journal of Pressure Vessel Technology*, Vol. 108, August 1986.
35. EPRI Report No. NP-5461, "Component Life Estimation: LWR Structural Material Degradation Mechanisms", September 1987, prepared by Structural Integrity Associates.



## **APPENDIX A**

**ASME Code Case N-481**

CASES OF ASME BOILER AND PRESSURE VESSEL CODE

Approval Date: March 5, 1990

See Numerical Index for expiration  
and any reaffirmation dates.

Case N-481

Alternative Examination Requirements for Cast  
Austenitic Pump Casings  
Section XI, Division 1

*Inquiry:* When conducting examination of cast austenitic pump casings in accordance with Section XI, Division 1, what examinations may be performed in lieu of the volumetric examinations specified in Table IWB-2500-1, Examination Category B-L-1, Item B12.10?

*Reply:* It is the opinion of the Committee that the following requirements shall be met in lieu of performing the volumetric examination specified in Table IWB-2500-1, Examination Category B-L-1, Item B12.10:

(a) Perform a VT-2 visual examination of the exterior of all pumps during the hydrostatic pressure test required by Table IWB-2500-1, Category B-P.

(b) Perform a VT-1 visual examination of the external surfaces of the weld of one pump casing.

(c) Perform a VT-3 visual examination of the internal surfaces whenever a pump is disassembled for maintenance.

(d) Perform an evaluation to demonstrate the safety and serviceability of the pump casing. The evaluation shall include the following:

(1) evaluating material properties, including fracture toughness values;

(2) performing a stress analysis of the pump casing;

(3) reviewing the operating history of the pump;

(4) selecting locations for postulating flaws;

(5) postulating one-quarter thickness reference flaw with a length six times its depth;

(6) establishing the stability of the selected flaw under the governing stress conditions;

(7) considering thermal aging embrittlement and any other processes that may degrade the properties of the pump casing during service.

(e) A report of this evaluation shall be submitted to the regulatory and enforcement authorities having jurisdiction at the plant site for review.



Docket Number 50-346  
License Number NPF-3  
Serial Number 2700  
Attachment 2  
Page 1 of 1

### **COMMITMENT LIST**

The following list identifies those actions committed to by the Davis-Besse Nuclear Power Station (DBNPS) in this document. Any other actions discussed in the submittal represent intended or planned actions the DBNPS. They are described only for information and are not regulatory commitments. Please notify the Manager - Regulatory Affairs (419-321-8450) at the DBNPS of any questions regarding this document or associated regulatory commitments.

#### **COMMITMENTS**

#### **DUE DATE**

None